 CMC, vol.57, no.3, pp.447-483, 2018

# A Size-Dependent Functionally Graded Higher Order Plate Analysis Based on Modified Couple Stress Theory and Moving Kriging Meshfree Method

**T. D. Tran[1], Chien H. Thai[2, 3, *] and H. Nguyen-Xuan[4, 5, *]**

**Abstract:** A size-dependent computational approach for bending, free vibration and buckling analyses of isotropic and sandwich functionally graded (FG) microplates is in this study presented. We consider both shear deformation and small scale effects through the generalized higher order shear deformation theory and modified couple stress theory (MCST). The present model only retains a single material length scale parameter for capturing properly size effects. A rule of mixture is used to model material properties varying through the thickness of plates. The principle of virtual work is used to derive the discrete system equations which are approximated by moving Kriging interpolation (MKI) meshfree method. Numerical examples consider the inclusions of geometrical parameters, volume fraction, boundary conditions and material length scale parameter. Reliability and effectiveness of the present method are confirmed through numerical results.

**Keywords:** Modified couple stress theory, isotropic and sandwich FGM plates, moving Kriging meshfree method.

## 1 Introduction

Nowadays, devices with small size have been widely used in various fields of aerospace, machinery, electronics and medical equipment. They have been also known as micro-electro-mechanical systems *(*MEMS) devices and are made of microbeam and microplate structures. Therefore, to use the devices effectively, an insight into mechanical behaviors of micro-structures are required. In addition, experimental studies indicate that the size effect takes into account in the micro-structures [Lam, Yang, Chong et al. (2003)]. Unfortunately, the classical continuum theories cannot enable to forecast exactly behaviors of micro-structures because of the insufficiency of material length scale

[1] Faculty of Construction & Electricity, Ho Chi Minh City Open University, Ho Chi Minh City, Vietnam.

[2] Division of Computational Mechanics, Ton Duc Thang University, Ho Chi Minh City, Vietnam.

[3] Faculty of Civil Engineering, Ton Duc Thang University, Ho Chi Minh City, Vietnam.

[4] Center for Interdisciplinary Research in Technology, Ho Chi Minh City University of Technology (HUTECH), Ho Chi Minh City, Vietnam.

[5] Department of Physical Therapy, Graduate Institute of Rehabilitation Science, China Medical University, Taichung, 40402, Taiwan.

[*] Corresponding Author: Chien H. Thai. Email: thaihoangchien@tdt.edu.vn;

H. Nguyen-Xuan. Email: ngx.hung@hutech.edu.vn.

parameters. Therefore, the advanced theories accounting higher order strain gradients named as the strain gradient theories taking into accounts additional material length scale parameters have been developed.

The strain gradient theories in the literature can be primarily categorized by two groups: The general strain gradient theory and the couple stress theory. The first one known as the general strain gradient theory proposed by Mindlin et al. [Mindlin and Eshel (1968); Mindlin (1964)], which are examined by all strain gradient components. This theory takes five material length-scale parameters into account in the classical material constants. However, it is hard to use in modeling and computation. For simplicity, the second theory [Toupin (1962); Mindlin and Tiersten (1962); Koiter (1964)] considered an anti-symmetric part of the strain gradient and included two material length scale parameters. In particular, a modified version of this theory known as the modified couple stress theory (MCST) was proposed by Yang et al. [Yang, Chong, Lam et al. (2002)]. It only involves a symmetric rotation gradient component and one material length scale parameter. At present, the MCST is highly interested in research community.

The MCST has been applied to FG microplates. A size-dependent three-dimensional (3D) elasticity model was early developed by Salehipour et al. [Salehipour, Nahvi, Shahidi et al. (2017)] for bending analysis of FG microplates. Guo et al. [Guo, Chen and Pan (2016); Guo, Chen and Pan (2017)] extended this approach to multilayered microplates. However, it is in fact for plate analysis that the size-dependent 3D elasticity model shows computationally too expensive. Tsiatas [Tsiatas (2009)] proposed then the Kirchhoff plate model for bending analysis of isotropic microplates. Several solutions based on this plate model were reported in Yin et al. [Yin, Qian, Wang et al. (2010); Jomehzadeh, Noori and Saidi (2011); Ansari and Norouzzadeh (2016)]. After that, a size-dependent first-order shear deformation plate theory (FSDT) based on the MCST was developed by Ma et al. [Ma, Gao and Reddy (2011)] for bending analysis and Ke et al. [Ke, Wang, Yang et al. (2012)] for free vibration analysis of isotropic microplates. Other relevant researches to this approach were also presented by Zhou et al. [Zhou and Gao (2014)] and Alinaghizadeh et al. [Alinaghizadeh, Shariati and Fish (2017)]. Moreover, a size-dependent third-order shear deformation (TSDT) model combined with the MSCT was developed by Gao et al. [Gao, Huang and Reddy (2013)] for isotropic microplates. After that, it was extended for FG microplates by Thai et al. [Thai and Kim (2013)] and Eshraghi et al. [Eshraghi, Dag and Soltani (2016)]. Thai et al. [Thai and Vo (2013)] proposed the sinusoidal plate model based on the MCST for FG microplates. Similarly, He et al. [He, Lou, Zhang et al. (2015)] and Lou et al. [Lou, He and Du (2015)] presented a size-dependent refined higher-order shear deformation (RPT) model for FG microplates. A size-dependent model accounting all shear and normal strains so-called the quasi-3D shear deformation theory was also proposed by Kim et al. [Kim and Reddy (2013)] for behavior analysis of FG microplates. The FSDT model was further developed for analysis of FG microplates [Lei, He, Zhang et al. (2015); Trinh, Vo, Thai et al. (2017); Nguyen, Nguyen, Wahab et al. (2017)].

For more details, Thai et al. [Thai, Vo, Nguyen et al. (2017)] presented a review of continuum mechanics models for size-dependent analysis of beams and plates. It showed that most size-dependent models developed rapidly in the last five years and

computational approaches herein were almost concerned with analytical methods. Addressing attempts to the advanced development of numerical methods such as finite elements, isogeometric analysis and meshfree for size-dependent analysis, we review a list of several studies in the literature. Phadikar et al. [Phadikar and Pradhan (2010)] presented a Kirchhoff finite element model based on the nonlocal elasticity theory for nanoplates. A FSDT finite element model combined with the nonlocal elasticity theory was reported by Ansari et al. [Ansari, Rajabiehfard and Arash (2010)]. Natarajan et al. [Natarajan, Chakraborty, Thangavel et al. (2012)] proposed a size-depedent isogeometric Mindlin plate model based on the nonlocal elasticity theory for nanoplates. Similarly, Nguyen et al. [Nguyen, Hui, Lee et al. (2015)] developed a size-dependent quasi-3D shear deformation model based on the nonlocal elasticity theory for FG nanoplates. An improved model by a combination of nonlocal and surface effects based on IGA was presented by Ansari et al. [Ansari and Norouzzadeh (2016)]. Besides, a size-dependent isogeometric model based on the modified strain gradient theory was proposed by Thai et al. [Thai, Ferreira and Nguyen (2018)] for analysis of FG microplates. Foroushani et al. [Sarrami-Foroushani and Azhari (2016)] and Mirsalehi et al. [Mirsalehi, Azhari and Amoushahi (2015)] developed the finite strip method incorporate with the nonlocal elasticity theory for FG nanoplates. Moreover, a size-dependent meshfree model based on the MCST for the isotropic microplates was developed by Roque et al. [Roque, Ferreira, and Reddy (2013)]. This model was applied for the FG microplates by Thai et al. [Thai, Ferreira, Lee et al. (2018)]. A further development of the meshfree method based on the nonlocal elasticity theory was presented by Zhang et al. [Zhang, Lei, Zhang et al. (2015)] for analysis of nanoplates. From above studies, it is clearly that a number of articles found in the literature based on the numerical solutions are still limited for analysis of micro/nano plates and shells [Rabczuk, Gracie, Song et al. (2010); Rabczuk, Areias and Belytschko (2007); Zenkour (2005)]. The above mention motivates us to develop a size-dependent HSDT meshfree model combined with the MCST for bending, free vibration and linear buckling analyses of isotropic and sandwich FG microplates.

The paper is outlined as follows. Basic equations of FG microplate based on the MCST are summarized in Section 2. In Section 3, FG microplate formulations based on moving Kriging interpolation are introduced. Numerical results are illustrated in Section 4. Finally, concluding remarks are given in Section 5.

## 2 Basic equations

### *2.1 Problem description*

#### *2.1.1 Isotropic FG plates*

As shown in Fig. 1, a FG microplate with thickness *h* made of a mixture of ceramic and metal is considered. Effective material parameters of the FG microplates as Young's modulus $(E)$, Poisson's ratio $(\nu)$ and density mass $(\rho)$ can be computed by a rule of mixture as:

$$E_e = (E_c - E_m)V(\mathrm{z}) + E_m;\ \ \nu_e = (\nu_c - \nu_m)V(\mathrm{z}) + \nu_m;\ \ \rho_e = (\rho_c - \rho_m)V(\mathrm{z}) + \rho_m \tag{1}$$

where the subscripts *c* and *m* define the ceramic and metal, respectively. $V(z)$ is the volume fraction of the constituents through the thickness by Reddy [Reddy (2000)]:

$$V(z)=\left(\frac{1}{2}+\frac{z}{h}\right)^{n};\ -\frac{h}{2}\le z\le\frac{h}{2} \tag{2}$$

in which the subscript *n* is the volume fraction exponent or the power index.

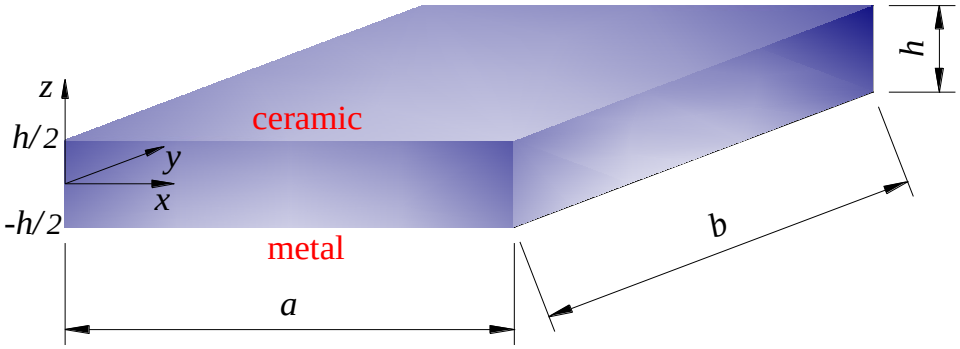


**Figure 1:** A typical configuration of FG microplate.

*2.1.2 Sandwich plates*

A sandwich FG microplate (cf. Fig. 2) made of a combination of an isotropic core and two FGM face sheets is considered, in which the bottom and top FGM sheets change from the metal-rich surface $\left(z=z_1\right)$ to the ceramic-rich surface $\left(z=z_2\right)$ and the ceramic-rich surface $\left(z=z_3\right)$ to the metal-rich surface $\left(z=z_4\right)$, respectively. The volume fraction of two face sheets are formed by a power-law function through the plate thickness given by Zenkour et al. [Zenkour (2005); Li, Lu and Kou (2008)]:

$$\begin{aligned}
&V(z)=\left(\frac{z-z_1}{z_2-z_1}\right)^{n},\ -\frac{h}{2}\le z\le z_2,\ \text{bottom layer}\\
&V(z)=1\quad,\quad z_2\le z\le z_3,\ \text{core layer}\\
&V(z)=\left(\frac{z_4-z}{z_4-z_3}\right)^{n},\ z_3\le z\le\frac{h}{2},\ \text{top layer}
\end{aligned} \tag{3}$$

Several types of the bottom-core-top thickness ratio $\left(h_b-h_c-h_t\right)$ are examined in this work. For example, $h_b-h_c-h_t=2-1-2$ indicates that the thickness of two face sheets are greater than two times compared to the core.


**Figure 2:** The sandwich plate with FGM sheets and homogeneous core

### *2.2 Modified couple stress theory*

The modified couple stress theory (MCST) [Yang, Chong, Lam et al. (2002)] regards one additional material length scale parameter in addition to the classical material constants instead of two ones as in the classical couple stress theory. The MCST additionally considers the symmetric rotation gradient tensor $\boldsymbol{\chi}$ into the strain tensor $\boldsymbol{\varepsilon}$. According to the MCST, the virtual strain energy $U$ in an isotropic linearly elastic material can be described by:

$$U = \int_V (\boldsymbol{\sigma} : \boldsymbol{\varepsilon} + \mathbf{m} : \boldsymbol{\chi}) \mathrm{d}V \tag{4}$$

where $\boldsymbol{\sigma}$ is the Cauchy stress tensor; $\mathbf{m}$ is high-order stress tensor corresponding with the rotation gradient tensors $\boldsymbol{\chi}$, respectively.

The relations of the strain tensor with displacement vector $\mathbf{u} = \{u \quad v \quad w\}^T$ and the rotation gradient tensor with rotation vector $\boldsymbol{\theta} = \{\theta_x \quad \theta_y \quad \theta_z\}^T$ are defined by

$$\boldsymbol{\varepsilon} = \frac{1}{2}\left[\nabla \mathbf{u} + (\nabla \mathbf{u})^T\right] \tag{5}$$

$$\boldsymbol{\chi} = \frac{1}{2}\left[\nabla \boldsymbol{\theta} + (\nabla \boldsymbol{\theta})^T\right] \tag{6}$$

where $\nabla$ ($\nabla = \left\{\frac{\partial}{\partial x} \quad \frac{\partial}{\partial y} \quad \frac{\partial}{\partial z}\right\}$) is the gradient operator.

The relation between displacement vector $\mathbf{u}$ and rotation vector $\boldsymbol{\theta}$ is expressed as follows

$$\boldsymbol{\theta}=\left\{\theta_x \quad \theta_y \quad \theta_z\right\}^T=\left\{\frac{1}{2}\left(\frac{\partial w}{\partial y}-\frac{\partial v}{\partial z}\right) \quad \frac{1}{2}\left(\frac{\partial u}{\partial z}-\frac{\partial w}{\partial x}\right) \quad \frac{1}{2}\left(\frac{\partial v}{\partial x}-\frac{\partial u}{\partial y}\right)\right\}^T \tag{7}$$

The constitutive relations are given by

$$\boldsymbol{\sigma}=\mathbf{C}\boldsymbol{\varepsilon} \tag{8}$$

$$\mathbf{m}=2G\ell^2\boldsymbol{\chi} \tag{9}$$

where **C,** $G$, $\ell$ are the stiffness tensor or elasticity tensor, the shear module and the material length scale parameter, respectively.

### *2.3 Kinematics of FG microplates*

A plate bounded by a domain $\mathbf{V}=\Omega\times\left(-\frac{h}{2},\frac{h}{2}\right)$ is considered, in which $\Omega\in\mathbb{R}^2$ and $h$ are the middle surface and the plate thickness, respectively. According to the generated higher order shear deformation theory [Thai, Ferreira, Rabczuk et al. (2014); Thai, Kulasegaram, Tran et al. (2014)], the displacement field of any points in the plate is formulated as follows:

$$\mathbf{u}(x,y,z)=\mathbf{u}^1(x,y)+z\mathbf{u}^2(x,y)+f(z)\mathbf{u}^3(x,y) \tag{10}$$

where

$$\mathbf{u}=\begin{Bmatrix}u\\v\\w\end{Bmatrix};\ \mathbf{u}^1=\begin{Bmatrix}u_0\\v_0\\w_0\end{Bmatrix};\ \mathbf{u}^2=-\begin{Bmatrix}w_{0,x}\\w_{0,y}\\0\end{Bmatrix};\ \mathbf{u}^3=\begin{Bmatrix}\beta_x\\\beta_y\\0\end{Bmatrix} \tag{11}$$

in which $u_0, v_0, w_0$, $\beta_x$ and $\beta_y$ are the in-plane, transverse displacements and the rotation components in the *y-z*, *x-z* planes, respectively. The symbols '*,x*' and '*,y*' indicates the derivative of arbitrary functions following *x* and *y* directions, respectively, and $f(z)$ is a certain function defined through plate thick.

Substituting Eq. (10) into Eq. (5), the strain components can be obtained by

$$\begin{aligned}&\varepsilon_{xx}=u_{0,x}-zw_{0,xx}+f(z)\beta_{x,x};\ \varepsilon_{yy}=v_{0,y}-zw_{0,yy}+f(z)\beta_{y,y};\\&\gamma_{xy}=u_{0,y}+v_{0,x}-2zw_{0,xy}+f(z)\left(\beta_{x,y}+\beta_{y,x}\right);\\&\gamma_{xz}=f'(z)\beta_x;\ \ \gamma_{yz}=f'(z)\beta_y;\ \varepsilon_{zz}=0\end{aligned} \tag{12}$$

The strains can be decomposed into two terms consisting of bending and shear strains which are expressed as follows

$$\boldsymbol{\varepsilon}=\left\{\varepsilon_{xx} \quad \varepsilon_{yy} \quad \gamma_{xy}\right\}^{\mathrm{T}}=\boldsymbol{\varepsilon}^1+z\boldsymbol{\varepsilon}^2+f(z)\boldsymbol{\varepsilon}^3 \ \text{ and } \ \boldsymbol{\gamma}=\left\{\gamma_{xz} \quad \gamma_{yz}\right\}^{\mathrm{T}}=f'(z)\boldsymbol{\varepsilon}^s \tag{13}$$

where

$$\boldsymbol{\varepsilon}^1=\begin{Bmatrix} u_{0,x} \\ v_{0,y} \\ u_{0,y}+v_{0,x} \end{Bmatrix};\ \boldsymbol{\varepsilon}^2=-\begin{Bmatrix} w_{0,xx} \\ w_{0,yy} \\ 2w_{0,xy} \end{Bmatrix};\ \boldsymbol{\varepsilon}^3=\begin{Bmatrix} \beta_{x,x} \\ \beta_{y,y} \\ \beta_{x,y}+\beta_{y,x} \end{Bmatrix};\ \boldsymbol{\varepsilon}^s=\begin{Bmatrix} \beta_x \\ \beta_y \end{Bmatrix} \tag{14}$$

in which $f'(z)$ is the derivation of the function $f(z)$. The function $f(z)$ can be determined so that transverse shear stresses corresponding with shear strains in Eq. (13) at top and bottom of microplates are equal to zeros or the value of its tangential at $z=\pm h/2$ is equal to zero.

Substituting Eq. (10) into Eq. (7), the rotation vector becomes

$$\begin{aligned}
\theta_x &= \frac{1}{2}\left(\frac{\partial w}{\partial y}-\frac{\partial v}{\partial z}\right)=\frac{1}{2}\left(2w_{0,y}-f'(z)\beta_y\right) \\
\theta_y &= \frac{1}{2}\left(\frac{\partial u}{\partial z}-\frac{\partial w}{\partial x}\right)=\frac{1}{2}\left(-2w_{0,x}+f'(z)\beta_x\right) \\
\theta_z &= \frac{1}{2}\left(\frac{\partial v}{\partial x}-\frac{\partial u}{\partial y}\right)=\frac{1}{2}\left(v_{0,x}-u_{0,y}\right)+\frac{1}{2}f'(z)\left(\beta_{y,x}-\beta_{x,y}\right)
\end{aligned} \tag{15}$$

Substituting Eq. (15) into Eq. (6), we write the symmetric rotation gradient as follows:

$$\begin{aligned}
&\chi^b_{xx}=\frac{\partial\theta_x}{\partial x}=\frac{1}{2}\left(2w_{0,xy}-f'(z)\beta_{y,x}\right);\ \chi^b_{yy}=\frac{\partial\theta_y}{\partial y}=\frac{1}{2}\left(-2w_{0,xy}+f'(z)\beta_{x,y}\right) \\
&\chi^b_{xy}=\frac{1}{2}\left(\frac{\partial\theta_x}{\partial y}+\frac{\partial\theta_y}{\partial x}\right)=\frac{1}{2}\left(w_{0,yy}-w_{0,yy}+-\frac{1}{2}f'(z)\left(\beta_{x,x}-\beta_{y,y}\right)\right); \\
&\chi^b_{zz}=\frac{\partial\theta_z}{\partial z}=\frac{1}{2}f'(z)\left(\beta_{y,x}-\beta_{x,y}\right) \\
&\chi^s_{xz}=\frac{1}{2}\left(\frac{\partial\theta_x}{\partial z}+\frac{\partial\theta_z}{\partial x}\right)=\frac{1}{4}\left(v_{o,xx}-u_{o,xy}\right)+\frac{1}{4}f(z)\left(\beta_{y,xx}-\beta_{x,xy}\right)-\frac{1}{4}f''(z)\beta_y; \\
&\chi^s_{yz}=\frac{1}{2}\left(\frac{\partial\theta_y}{\partial z}+\frac{\partial\theta_z}{\partial y}\right)=\frac{1}{4}\left(v_{o,xy}-u_{o,yy}\right)+\frac{1}{4}f(z)\left(\beta_{y,xy}-\beta_{x,yy}\right)-\frac{1}{4}f''(z)\beta_x
\end{aligned} \tag{16}$$

The symmetric rotation gradient tensor can be rewritten under a compact form by

$$\boldsymbol{\chi}=\begin{Bmatrix} \boldsymbol{\chi}^b \\ \boldsymbol{\chi}^s \end{Bmatrix},$$

where $\boldsymbol{\chi}^b=\left\{\chi^b_{xx}\quad\chi^b_{yy}\quad\chi^b_{xy}\quad\chi^b_{zz}\right\}^T=\boldsymbol{\chi}^b_1+f'(z)\boldsymbol{\chi}^b_2;$ (17)

$$\boldsymbol{\chi}^s=\begin{Bmatrix} \chi^s_{xz} \\ \chi^s_{yz} \end{Bmatrix}=\boldsymbol{\chi}^s_1+f(z)\boldsymbol{\chi}^s_2+f''(z)\boldsymbol{\chi}^s_3$$

and

$$\boldsymbol{\chi}_1^b=\begin{Bmatrix} w_{0,xy} \\ -w_{0,xy} \\ \frac{1}{2}\left(w_{0,yy}-w_{0,xx}\right) \\ 0 \end{Bmatrix};\ \boldsymbol{\chi}_2^b=\begin{Bmatrix} -\frac{1}{2}\beta_{y,x} \\ \frac{1}{2}\beta_{x,y} \\ \frac{1}{4}\left(\beta_{x,x}-\beta_{y,y}\right) \\ \frac{1}{2}\left(\beta_{y,x}-\beta_{x,y}\right) \end{Bmatrix};$$

$$\boldsymbol{\chi}_1^s=\frac{1}{4}\begin{Bmatrix} v_{0,xx}-u_{0,xy} \\ v_{0,xy}-u_{0,yy} \end{Bmatrix};\ \boldsymbol{\chi}_2^s=\frac{1}{4}\begin{Bmatrix} \beta_{y,xx}-\beta_{x,xy} \\ \beta_{y,xy}-\beta_{x,yy} \end{Bmatrix};\ \boldsymbol{\chi}_3^s=\frac{1}{4}\begin{Bmatrix} -\beta_y \\ \beta_x \end{Bmatrix} \tag{18}$$

The classical and modified couple stress linear elastic constitutive relations are written as follows

$$\begin{Bmatrix} \sigma_{xx} \\ \sigma_{yy} \\ \tau_{xy} \\ \tau_{xz} \\ \tau_{yz} \end{Bmatrix}=\begin{bmatrix} Q_{11} & Q_{12} & 0 & 0 & 0 \\ Q_{21} & Q_{22} & 0 & 0 & 0 \\ 0 & 0 & Q_{66} & 0 & 0 \\ 0 & 0 & 0 & Q_{55} & 0 \\ 0 & 0 & 0 & 0 & Q_{44} \end{bmatrix}\begin{Bmatrix} \varepsilon_{xx} \\ \varepsilon_{yy} \\ \gamma_{xy} \\ \gamma_{xz} \\ \gamma_{yz} \end{Bmatrix} \tag{19}$$

$$\begin{Bmatrix} m_{xx} \\ m_{yy} \\ m_{xy} \\ m_{zz} \\ m_{xz} \\ m_{yz} \end{Bmatrix}=2Gl_1^2\begin{bmatrix} 1 & 0 & 0 & 0 & 0 & 0 \\ 0 & 1 & 0 & 0 & 0 & 0 \\ 0 & 0 & 1 & 0 & 0 & 0 \\ 0 & 0 & 0 & 1 & 0 & 0 \\ 0 & 0 & 0 & 0 & 1 & 0 \\ 0 & 0 & 0 & 0 & 0 & 1 \end{bmatrix}\begin{Bmatrix} \chi_{xx} \\ \chi_{yy} \\ \chi_{xy} \\ \chi_{zz} \\ \chi_{xz} \\ \chi_{yz} \end{Bmatrix} \tag{20}$$

where

$$Q_{11}=Q_{22}=\frac{E_e}{1-\nu_e^2},\ Q_{12}=Q_{21}=\frac{\nu_e E_e}{1-\nu_e^2},\ Q_{66}=Q_{55}=Q_{44}=\frac{E_e}{2(1+\nu_e)},\ G=\frac{E_e}{2(1+\nu_e)} \tag{21}$$

where $E_e$ and $\nu_e$ are the effective Young module and Poisson's ratio according to Eq. (1), respectively.

The discrete Galerkin weak form for the bending analysis of the FG microplate subjected to a transverse loading $q_0$ are written by

$$\int_{\Omega}\int_{-h/2}^{h/2}\left(\sigma_{xx}\delta\varepsilon_{xx}+\sigma_{yy}\delta\varepsilon_{yy}+\tau_{xy}\delta\gamma_{xy}+\tau_{xz}\delta\gamma_{xz}+\tau_{yz}\delta\gamma_{yz}\right)\mathrm{d}\Omega\mathrm{d}z+$$
$$\int_{\Omega}\int_{-h/2}^{h/2}\left(m_{xx}\delta\chi_{xx}+m_{yy}\delta\chi_{yy}+m_{zz}\delta\chi_{zz}+2m_{xy}\delta\chi_{xy}+2m_{xz}\delta\chi_{xz}+2m_{yz}\delta\chi_{yz}\right)\mathrm{d}\Omega\mathrm{d}z=\int_{\Omega}\delta w_0 q_0\mathrm{d}\Omega \tag{22}$$

The Eq. (22) can split into two independent integrals following to middle surface and *z*-axis direction. Substituting Eq. (19) and Eq. (20) into Eq. (22), the discrete Galerkin weak form can be rewritten under the matrix form as follows

$$\int_{\Omega}\delta\hat{\boldsymbol{\varepsilon}}^{T}\hat{\mathbf{D}}\hat{\boldsymbol{\varepsilon}}\mathrm{d}\Omega+\int_{\Omega}\delta\left(\boldsymbol{\varepsilon}^{s}\right)^{T}\mathbf{D}^{s}\boldsymbol{\varepsilon}^{s}\mathrm{d}\Omega+\int_{\Omega}\delta\left(\hat{\boldsymbol{\chi}}^{b}\right)^{T}\hat{\mathbf{D}}_{c}^{b}\hat{\boldsymbol{\Gamma}}_{c}^{b}\hat{\boldsymbol{\chi}}^{b}\mathrm{d}\Omega+\int_{\Omega}\delta\left(\hat{\boldsymbol{\chi}}^{s}\right)^{T}\hat{\mathbf{D}}_{c}^{s}\hat{\boldsymbol{\Gamma}}_{c}^{s}\hat{\boldsymbol{\chi}}^{s}\mathrm{d}\Omega=\int_{\Omega}\delta w_0 q_0\mathrm{d}\Omega \tag{23}$$

where

$$\hat{\boldsymbol{\varepsilon}}=\left\{\boldsymbol{\varepsilon}_1\quad\boldsymbol{\varepsilon}_2\quad\boldsymbol{\varepsilon}_3\right\}^{T};\ \hat{\boldsymbol{\chi}}^{b}=\left\{\boldsymbol{\chi}_1^{b}\quad\boldsymbol{\chi}_2^{b}\right\};\ \hat{\boldsymbol{\chi}}^{s}=\left\{\boldsymbol{\chi}_1^{s}\quad\boldsymbol{\chi}_2^{s}\quad\boldsymbol{\chi}_3^{s}\right\}^{T};$$
$$\hat{\mathbf{D}}=\begin{bmatrix}\mathbf{A}^{b}&\mathbf{B}^{b}&\mathbf{E}^{b}\\ \mathbf{B}^{b}&\mathbf{D}^{b}&\mathbf{F}^{b}\\ \mathbf{E}^{b}&\mathbf{F}^{b}&\mathbf{H}^{b}\end{bmatrix};\ \hat{\mathbf{D}}_{c}^{b}=\begin{bmatrix}\mathbf{A}_{c}^{b}&\mathbf{B}_{c}^{b}\\ \mathbf{B}_{c}^{b}&\mathbf{D}_{c}^{b}\end{bmatrix};\ \hat{\mathbf{D}}_{c}^{s}=\begin{bmatrix}\mathbf{A}_{c}^{s}&\mathbf{B}_{c}^{s}&\mathbf{E}_{c}^{s}\\ \mathbf{B}_{c}^{s}&\mathbf{D}_{c}^{s}&\mathbf{F}_{c}^{s}\\ \mathbf{E}_{c}^{s}&\mathbf{F}_{c}^{s}&\mathbf{H}_{c}^{s}\end{bmatrix}; \tag{24}$$
$$\hat{\boldsymbol{\Gamma}}_{c}^{b}=\begin{bmatrix}\boldsymbol{\Gamma}_{c}^{b}&0\\ 0&\boldsymbol{\Gamma}_{c}^{b}\end{bmatrix};\ \hat{\boldsymbol{\Gamma}}_{c}^{s}=\begin{bmatrix}\boldsymbol{\Gamma}_{c}^{s}&0&0\\ 0&\boldsymbol{\Gamma}_{c}^{s}&0\\ 0&0&\boldsymbol{\Gamma}_{c}^{s}\end{bmatrix};\ \boldsymbol{\Gamma}_{c}^{b}=diag\left(1,1,2,1\right);\ \boldsymbol{\Gamma}_{c}^{b}=diag\left(2,2\right)$$

in which

$$\left(\mathbf{A}^{b},\mathbf{B}^{b},\mathbf{D}^{b},\mathbf{E}^{b},\mathbf{F}^{b},\mathbf{H}^{b}\right)=\int_{-h/2}^{h/2}\left(1,z,z^{2},f(z),z\,f(z),f^{2}(z)\right)\begin{bmatrix}Q_{11}&Q_{12}&0\\ Q_{21}&Q_{22}&0\\ 0&0&Q_{66}\end{bmatrix}\mathrm{d}z;$$
$$\mathbf{D}^{s}=\int_{-h/2}^{h/2}f'^{2}(z)\begin{bmatrix}Q_{44}&0\\ 0&Q_{55}\end{bmatrix}\mathrm{d}z;\ \left(\mathbf{A}_{c}^{b},\mathbf{B}_{c}^{b},\mathbf{D}_{c}^{b}\right)=\int_{-h/2}^{h/2}2Gl^{2}\left(1,f'(z),(f'(z))^{2}\right)\mathbf{I}_{4x4}\mathrm{d}z; \tag{25}$$
$$\left(\mathbf{A}_{c}^{s},\mathbf{B}_{c}^{s},\mathbf{D}_{c}^{s},\mathbf{E}_{c}^{s},\mathbf{F}_{c}^{s},\mathbf{H}_{c}^{s}\right)=\int_{-h/2}^{h/2}2Gl^{2}\left(1,f(z),(f(z))^{2},f''(z),f(z)f''(z),(f''(z))^{2}\right)\mathbf{I}_{2x2}\mathrm{d}z$$

in which $\mathbf{I}_{2x2}$, $\mathbf{I}_{4x4}$ are identity matrices of size 2×2 and 4×4, respectively.

The discrete Galerkin weak form for free vibration analysis of the FG microplate can also be defined by:

$$\int_{\Omega}\delta\hat{\boldsymbol{\varepsilon}}^{T}\hat{\mathbf{D}}\hat{\boldsymbol{\varepsilon}}\mathrm{d}\Omega+\int_{\Omega}\delta\left(\boldsymbol{\varepsilon}^{s}\right)^{T}\mathbf{D}^{s}\boldsymbol{\varepsilon}^{s}\mathrm{d}\Omega+\int_{\Omega}\delta\left(\hat{\boldsymbol{\chi}}^{b}\right)^{T}\hat{\mathbf{D}}_{c}^{b}\hat{\boldsymbol{\Gamma}}_{c}^{b}\hat{\boldsymbol{\chi}}^{b}\mathrm{d}\Omega+\int_{\Omega}\delta\left(\hat{\boldsymbol{\chi}}^{s}\right)^{T}\hat{\mathbf{D}}_{c}^{s}\hat{\boldsymbol{\Gamma}}_{c}^{s}\hat{\boldsymbol{\chi}}^{s}\mathrm{d}\Omega+\int_{\Omega}\delta\hat{\mathbf{u}}^{T}\hat{\mathbf{m}}\ddot{\hat{\mathbf{u}}}\mathrm{d}\Omega=\mathbf{0} \tag{26}$$

where

$$\hat{\mathbf{u}}=\begin{Bmatrix}\mathbf{u}^1\\ \mathbf{u}^2\\ \mathbf{u}^3\end{Bmatrix};\ \hat{\mathbf{m}}=\begin{bmatrix}\mathbf{I}_1 & \mathbf{I}_2 & \mathbf{I}_4\\ \mathbf{I}_2 & \mathbf{I}_3 & \mathbf{I}_5\\ \mathbf{I}_4 & \mathbf{I}_5 & \mathbf{I}_6\end{bmatrix};\ (\mathbf{I}_1,\mathbf{I}_2,\mathbf{I}_3,\mathbf{I}_4,\mathbf{I}_5,\mathbf{I}_6)=\int_{-h/2}^{h/2}\rho_e\left(1,z,z^2,f(z),zf(z),f^2(z)\right)\begin{bmatrix}1&0&0\\0&1&0\\0&0&1\end{bmatrix}\mathrm{d}z \tag{27}$$

The discrete Galerkin weak form for buckling analysis of the FG microplate under an in-plane loading can be expressed by:

$$\int_\Omega \delta\hat{\boldsymbol{\varepsilon}}^T\hat{\mathbf{D}}\hat{\boldsymbol{\varepsilon}}\mathrm{d}\Omega+\int_\Omega\delta\left(\boldsymbol{\varepsilon}^s\right)^T\mathbf{D}^s\boldsymbol{\varepsilon}^s\mathrm{d}\Omega+\int_\Omega\delta\left(\hat{\boldsymbol{\chi}}^b\right)^T\hat{\mathbf{D}}_c^b\hat{\boldsymbol{\Gamma}}_c^b\hat{\boldsymbol{\chi}}^b\mathrm{d}\Omega+\int_\Omega\delta\left(\hat{\boldsymbol{\chi}}^s\right)^T\hat{\mathbf{D}}_c^s\hat{\boldsymbol{\Gamma}}_c^s\hat{\boldsymbol{\chi}}^s\mathrm{d}\Omega+$$
$$h\int_\Omega\delta\begin{Bmatrix}w_{0,x}\\w_{0,y}\end{Bmatrix}^{\mathrm{T}}\begin{bmatrix}N_x^0 & N_{xy}^0\\ N_{xy}^0 & N_y^0\end{bmatrix}\begin{Bmatrix}w_{0,x}\\w_{0,y}\end{Bmatrix}\mathrm{d}\Omega=\mathbf{0} \tag{28}$$

where $N_x^0$ and $N_y^0$ are pre-buckling loads in *x*, *y* directions, respectively; $N_{xy}^0$ is a plane shear load in *x*-*y* surface.

## 3 FG microplate formulation based on moving Kriging interpolation

### *3.1 Moving Kriging interpolation shape functions*

Let us consider a given domain $\Omega$ which is discretized into a set of nodes $\mathbf{x}_I$ ($I$ = 1,..., *NP*), as shown in Fig. 3, in which *NP* denotes the number of nodes in the problem domain. According to the moving Kriging shape functions, the displacement field $u^h(\mathbf{x})$ is described by

$$u^h(\mathbf{x})=\sum_{I=1}^{NP}N_I(\mathbf{x})u_I \tag{29}$$

where $u_I$ is the unknown coefficient associated with node $I$ and $N_I$ is the moving Kriging shape function being expressed as follows

$$N_I(\mathbf{x})=\sum_{j=1}^{m}p_j(\mathbf{x})A_{jI}+\sum_{k=1}^{n}r_k(\mathbf{x})B_{kI}\quad\text{or}\quad N_I(\mathbf{x})=\mathbf{p}^{\mathrm{T}}(\mathbf{x})\mathbf{A}+\mathbf{r}^{\mathrm{T}}(\mathbf{x})\mathbf{B} \tag{30}$$

in which $n$ is a number of nodes in a support domain $\Omega_x\in\Omega$ and $m$ is the dimension of a polynomial basis function space. In addition, $\mathbf{A}$, $\mathbf{B}$, $\mathbf{p}(\mathbf{x})$ and $\mathbf{r}(\mathbf{x})$ are expressed as:

$$\mathbf{A}=(\mathbf{P}^{\mathrm{T}}\mathbf{R}^{-1}\mathbf{P})^{-1}\mathbf{P}^{\mathrm{T}}\mathbf{R}^{-1},\ \mathbf{B}=\mathbf{R}^{-1}(\mathbf{I}-\mathbf{PA})$$
$$\mathbf{p}(\mathbf{x})=\begin{Bmatrix}1 & x & y & x^2 & xy & y^2 & ...\end{Bmatrix}^T\text{ and} \tag{31}$$
$$\mathbf{r}(\mathbf{x})=[\,R(\mathbf{x}_1,\mathbf{x})\quad R(\mathbf{x}_2,\mathbf{x})\quad\cdots\quad R(\mathbf{x}_n,\mathbf{x})\,]^{\mathrm{T}}$$

where $\mathbf{I}$ is the identity matrix of size $n\times n$.

According to the discrete Galerkin weak form, a minimum choice of $\mathbf{p}(\mathbf{x})$ is the quadratic polynomial functions:

$$\mathbf{p}(\mathbf{x})=\begin{Bmatrix}1 & x & y & x^2 & xy & y^2\end{Bmatrix}^T\ (m=6) \tag{32}$$

Now we write $\mathbf{P}$ and $\mathbf{R}$ as follows

$$\mathbf{P}=\begin{bmatrix} p_1(\mathbf{x}_1) & \dots & p_m(\mathbf{x}_1) \\ \dots & \dots & \dots \\ p_1(\mathbf{x}_n) & \dots & p_m(\mathbf{x}_n) \end{bmatrix} \text{ and } \mathbf{R}=\begin{bmatrix} R(\mathbf{x}_1,\mathbf{x}_1) & \dots & R(\mathbf{x}_1,\mathbf{x}_n) \\ \dots & \dots & \dots \\ R(\mathbf{x}_n,\mathbf{x}_1) & \dots & R(\mathbf{x}_n,\mathbf{x}_n) \end{bmatrix} \tag{33}$$

where $R(\mathbf{x}_I,\mathbf{x}_J)=\frac{1}{2}E\left[\left(u^h(\mathbf{x}_I)-u^h(\mathbf{x}_J)\right)^2\right]$ is a correlation function, in which $E$ denotes an expected value of a random function.

Various correlation functions consisting of multi-quadrics, thin plate splines, Gaussian can be chosen to construct MKI shape functions. For example, the Gaussian function can be utilized and it is defined as

$$R(\mathbf{x}_I,\mathbf{x}_J)=\mathrm{e}^{-\left(\frac{\beta r_{IJ}}{a_0}\right)^2} \tag{34}$$

where $r_{IJ}=\left\|\mathbf{x}_I-\mathbf{x}_J\right\|$, the correlation parameter $\beta$ is related to the variance $\sigma^2$ of the normal distribution function by $\beta^2=1/2\sigma^2$. The scale factor $a_0$ stands for the normalized distance. For regularly distributed nodes, $a_0$ is taken as the length of two adjacent nodes, and it is chosen to be the maximum distance between a pair of nodes in the support domain for the irregularly distributed nodes. The previous works [Thai, Do and Nguyen-Xuan (2016); Thai, Nguyen, Rabczuk et al. (2016); Nguyen, Thai and Nguyen-Xuan (2016); Phan-Dao, Thai, Lee et al. (2016); Thai, Ferreira and Nguyen-Xuan (2017); Thai, Ferreira, Rabczuk et al. (2018)] showed that the normalized correlation function is stable and not influenced by the correlation parameter $\beta$. Hence, the correlation parameter is assumed to be equal to 1.

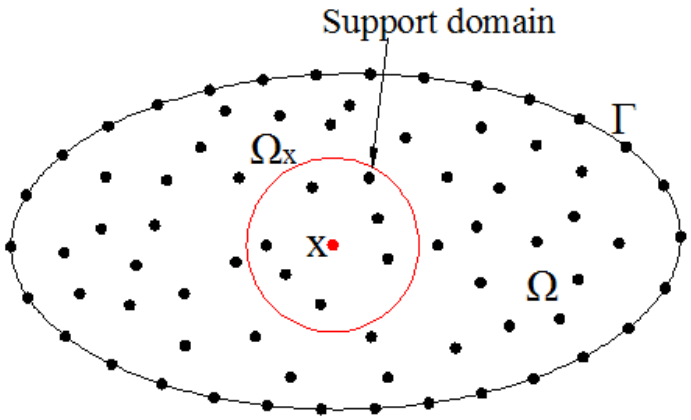


**Figure 3:** Domain representation and support domain of 2D model

The first and second-order derivatives of the MKI shape functions are expressed by

$$N_{I,x}(\mathbf{x})=\sum_{j=1}^{m}p_{j,x}(\mathbf{x})A_{jI}+\sum_{k=1}^{n}r_{k,x}(\mathbf{x})B_{kI};\ N_{I,y}(\mathbf{x})=\sum_{j=1}^{m}p_{j,y}(\mathbf{x})A_{jI}+\sum_{k=1}^{n}r_{k,y}(\mathbf{x})B_{kI};$$
$$N_{I,xx}(\mathbf{x})=\sum_{j=1}^{m}p_{j,xx}(\mathbf{x})A_{jI}+\sum_{k=1}^{n}r_{k,xx}(\mathbf{x})B_{kI};\ \ N_{I,yy}(\mathbf{x})=\sum_{j=1}^{m}p_{j,yy}(\mathbf{x})A_{jI}+\sum_{k=1}^{n}r_{k,yy}(\mathbf{x})B_{kI};\tag{35}$$
$$N_{I,xy}(\mathbf{x})=\sum_{j=1}^{m}p_{j,xy}(\mathbf{x})A_{jI}+\sum_{k=1}^{n}r_{k,xy}(\mathbf{x})B_{kI}$$

In meshfree methods, a support domain of nodes is needed to construct the shape functions. Herein, the size of the support domain is important and can be defined as

$$d_m=\alpha d_c\tag{36}$$

where $d_c$ and $\alpha$ are an average distance between nodes and a scale factor, respectively. It is shown that the size of the support domain is enough large to support a sufficient number of nodes for achievement of stable solutions. Such a value of scale factor can be determined through numerical experience.

### *3.2 A MKI-based formulation using the HSDT and modified couple stress theory*

According to the MK interpolation, the displacement field can be approximated as

$$\mathbf{u}^h(x,y)=\sum_{I=1}^{n}\begin{bmatrix}N_I(x,y)&0&0&0&0\\0&N_I(x,y)&0&0&0\\0&0&N_I(x,y)&0&0\\0&0&0&N_I(x,y)&0\\0&0&0&0&N_I(x,y)\end{bmatrix}\begin{Bmatrix}u_{0I}\\v_{0I}\\w_{0I}\\\beta_{xI}\\\beta_{yI}\end{Bmatrix}=\sum_{I=1}^{n}\mathbf{N}_I(x,y)\mathbf{q}_I\tag{37}$$

where $\mathbf{q}_I=\begin{Bmatrix}u_{0I}&v_{0I}&w_{0I}&\beta_{xI}&\beta_{yI}\end{Bmatrix}^T$ is a vector that contains degrees of freedom of node *I*.

Substituting Eq. (36) into Eq. (14), the strain components can be rewritten as

$$\hat{\boldsymbol{\varepsilon}}=\begin{Bmatrix}\boldsymbol{\varepsilon}^1&\boldsymbol{\varepsilon}^2&\boldsymbol{\varepsilon}^3\end{Bmatrix}^T=\sum_{I=1}^{n}\begin{Bmatrix}\mathbf{B}_I^1&\mathbf{B}_I^2&\mathbf{B}_I^3\end{Bmatrix}^T\mathbf{q}_I=\sum_{I=1}^{n}\hat{\mathbf{B}}_I\mathbf{q}_I;\ \ \boldsymbol{\varepsilon}^s=\sum_{I=1}^{n}\mathbf{B}_I^s\mathbf{q}_I\tag{38}$$

in which,

$$\mathbf{B}_I^1=\begin{bmatrix}N_{I,x}&0&0&0&0\\N_{I,x}&N_{I,y}&0&0&0\\N_{I,y}&0&0&0&0\end{bmatrix};\quad \mathbf{B}_I^2=-\begin{bmatrix}0&0&N_{I,xx}&0&0\\0&0&N_{I,yy}&0&0\\0&0&2N_{I,xy}&0&0\end{bmatrix};$$
$$\mathbf{B}_I^3=\begin{bmatrix}0&0&0&N_{I,x}&0\\0&0&0&0&N_{I,y}\\0&0&0&N_{I,y}&N_{I,x}\end{bmatrix};\quad \mathbf{B}_I^s=\begin{bmatrix}0&0&0&N_I&0\\0&0&0&0&N_I\end{bmatrix}\tag{39}$$

Similarly, the rotation gradient components are obtained by substituting Eq. (36) into Eq. (18) as follows

$$\begin{aligned}\hat{\boldsymbol{\chi}}^b &= \left\{\boldsymbol{\chi}_1^b \quad \boldsymbol{\chi}_2^b\right\}^T = \sum_{I=1}^{n}\left\{\mathbf{B}_{cI}^{b1} \quad \mathbf{B}_{cI}^{b2}\right\}^T \mathbf{q}_I = \sum_{I=1}^{n}\hat{\mathbf{B}}_{cI}^b\mathbf{q}_I \\ \hat{\boldsymbol{\chi}}^s &= \left\{\boldsymbol{\chi}_1^s \quad \boldsymbol{\chi}_2^s \quad \boldsymbol{\chi}_3^s\right\}^T = \sum_{I=1}^{n}\left\{\mathbf{B}_{cI}^{s1} \quad \mathbf{B}_{cI}^{s2} \quad \mathbf{B}_{cI}^{s3}\right\}^T \mathbf{q}_I = \sum_{I=1}^{n}\hat{\mathbf{B}}_{cI}^s\mathbf{q}_I\end{aligned} \tag{40}$$

in which,

$$\mathbf{B}_{cI}^{b1} = \begin{bmatrix} 0 & 0 & N_{I,xy} & 0 & 0 \\ 0 & 0 & -N_{I,xy} & 0 & 0 \\ 0 & 0 & \frac{1}{2}\left(N_{I,yy} - N_{I,xx}\right) & 0 & 0 \\ 0 & 0 & 0 & 0 & 0 \end{bmatrix};\ \mathbf{B}_{cI}^{b2} = \begin{bmatrix} 0 & 0 & 0 & 0 & -\frac{1}{2}N_{I,x} \\ 0 & 0 & 0 & \frac{1}{2}N_{I,y} & 0 \\ 0 & 0 & 0 & \frac{1}{2}N_{I,x} & -\frac{1}{2}N_{I,y} \\ 0 & 0 & 0 & -\frac{1}{2}N_{I,y} & \frac{1}{2}N_{I,x} \end{bmatrix}; \tag{41}$$

$$\mathbf{B}_{cI}^{s1} = \frac{1}{4}\begin{bmatrix} -N_{I,xy} & N_{I,xx} & 0 & 0 & 0 \\ -N_{I,yy} & N_{I,xy} & 0 & 0 & 0 \end{bmatrix};\ \mathbf{B}_{cI}^{s2} = \frac{1}{4}\begin{bmatrix} 0 & 0 & 0 & -N_{I,xy} & N_{I,xx} \\ 0 & 0 & 0 & -N_{I,yy} & N_{I,xy} \end{bmatrix};$$

$$\mathbf{B}_{cI}^{s3} = \frac{1}{4}\begin{bmatrix} 0 & 0 & 0 & 0 & -N_I \\ 0 & 0 & 0 & N_I & 0 \end{bmatrix}$$

Substituting Eq. (36) into Eq. (11), the displacement fields $\mathbf{u}^1$, $\mathbf{u}^2$ and $\mathbf{u}^3$ can be expressed as follows

$$\hat{\mathbf{u}} = \left\{\mathbf{u}^1 \quad \mathbf{u}^2 \quad \mathbf{u}^3\right\}^T = \sum_{I=1}^{n}\left\{\mathbf{N}_I^1 \quad \mathbf{N}_I^2 \quad \mathbf{N}_I^3\right\}^T \mathbf{q}_I = \sum_{I=1}^{n}\hat{\mathbf{N}}\mathbf{q}_I \tag{42}$$

where

$$\mathbf{N}_I^1 = \begin{bmatrix} N_I & 0 & 0 & 0 & 0 \\ 0 & N_I & 0 & 0 & 0 \\ 0 & 0 & N_I & 0 & 0 \end{bmatrix};\ \mathbf{N}_I^2 = -\begin{bmatrix} 0 & 0 & N_{I,x} & 0 & 0 \\ 0 & 0 & N_{I,y} & 0 & 0 \\ 0 & 0 & 0 & 0 & 0 \end{bmatrix} \text{ and } \mathbf{N}_I^3 = \begin{bmatrix} 0 & 0 & 0 & N_I & 0 \\ 0 & 0 & 0 & 0 & N_I \\ 0 & 0 & 0 & 0 & 0 \end{bmatrix} \tag{43}$$

The derivatives of transverse bending and shear displacements are also given by

$$\begin{Bmatrix} w_{0,x} \\ w_{0,y} \end{Bmatrix} = \sum_{I=1}^{n}\begin{bmatrix} 0 & 0 & N_{I,x} & 0 & 0 \\ 0 & 0 & N_{I,y} & 0 & 0 \end{bmatrix}\mathbf{q}_I = \sum_{I=1}^{n}\mathbf{B}_I^g\mathbf{q}_I \tag{44}$$

Substituting Eqs. (37), (39), (41) and (43) into Eqs. (23), (26) and (27), we obtain the equations system of the static, free vibration and buckling analyses of FG microplates as

$$\mathbf{Kq} = \mathbf{F} \tag{45}$$

$$\left(\mathbf{K} - \omega^2\mathbf{M}\right)\mathbf{q} = \mathbf{0} \tag{46}$$

$$\left(\mathbf{K}-\lambda_{cr}\mathbf{K}^{g}\right)\mathbf{q}=\mathbf{0} \tag{47}$$

where $\mathbf{K}$ ( $\mathbf{K}=\mathbf{K}^{\varepsilon}+\mathbf{K}^{\theta}$ ), $\mathbf{M}$ , $\mathbf{K}^{g}$ and $\mathbf{F}$ are the global stiffness matrix, mass matrix, geometry stiffness matrix and force vector, respectively, in which:

$$\begin{aligned}
&\mathbf{K}^{\varepsilon}=\int_{\Omega}\hat{\mathbf{B}}^{T}\hat{\mathbf{D}}\hat{\mathbf{B}}\Omega+\int_{\Omega}\left(\mathbf{B}^{s}\right)^{T}\mathbf{D}^{s}\mathbf{B}^{s}\mathrm{d}\Omega;\\
&\mathbf{K}^{\theta}=\int_{\Omega}\left(\hat{\mathbf{B}}_{c}^{b}\right)^{T}\hat{\mathbf{D}}_{c}^{b}\hat{\Gamma}_{c}^{b}\hat{\mathbf{B}}_{c}^{b}\mathrm{d}\Omega+\int_{\Omega}\left(\hat{\mathbf{B}}_{c}^{s}\right)^{T}\hat{\mathbf{D}}_{c}^{s}\hat{\Gamma}_{c}^{s}\hat{\mathbf{B}}_{c}^{s}\mathrm{d}\Omega;\\
&\mathbf{F}=\int_{\Omega}q_{0}\left\{0\quad 0\quad N_{I}\quad 0\quad 0\right\}^{\mathrm{T}}\mathrm{d}\Omega;\quad \mathbf{M}=\int_{\Omega}\hat{\mathbf{N}}^{T}\mathbf{I}_{m}\hat{\mathbf{N}}\mathrm{d}\Omega;\\
&\mathbf{K}^{g}=h\int_{\Omega}\left(\mathbf{B}^{g}\right)^{\mathrm{T}}\begin{bmatrix}N_{x}^{0} & N_{xy}^{0}\\ N_{xy}^{0} & N_{y}^{0}\end{bmatrix}\mathbf{B}^{g}\mathrm{d}\Omega
\end{aligned} \tag{48}$$

and $\omega$ and $\lambda_{cr}$ in Eq. (45) and Eq. (46) are the natural frequency and the critical buckling load, respectively.

## 4 Numerical examples and discussions

To start with numerical analysis, material properties are given in Tab. 1. Without loss of generality, the cubic distribution function [Reddy (2000)] is used. In addition, a background cell with 4×4 Gauss points for each cell is used for numerical computation. The material length scale factor ($l$=17.6×10$^{-6}$ m) [Lam, Yang, Chong et al. (2003)] is adopted in numerical examples. Also, homogeneous Dirichlet boundary conditions (BCs) are considered as follows:

- Simply supported:
  - Rectangular plate

    $u_0=w_0=\beta_x=0$ at $y=0,b$ and $v_0=w_0=\beta_y=0$ at $x=0,a$
  - Circular plate

    $w_0=0$ at boundaries
- Fully clamped:

  $u_0=v_0=w_0=\beta_x=\beta_y=w_{0,x}=w_{0,y}=0$ at boundaries

The BCs for $u_0, v_0, w_0, \beta_x, \beta_y$ are enforced as the similar way to the traditional finite element method, while the derivation of displacements $w_{0,x}, w_{0,y}$ is eliminated by assigning zero values of the transverse and shear displacements at boundary nodes and its adjacent nodes as same as the previous studies [Nguyen, Ngo and Nguyen-Xuan (2017); Nguyen-Thanh, Zhou, Zhuang et al. (2017)]. In addition, the essential boundary conditions for the derivation of transverse and shear displacements into the MK meshfree method are simply implemented without use of any additional variables.

For comparison purpose, non-dimensional displacement, natural frequency and critical buckling load of the FG microplate are defined by:

- The isotropic FG rectangular microplate:

$$\bar{w} = \frac{10h^3 E_c}{\bar{q}_0 a^4} w\left(\frac{a}{2}, \frac{b}{2}\right);\ \bar{\omega} = \omega h\sqrt{\frac{\rho_c}{E_c}};\ \bar{\lambda}_{cr} = \frac{\lambda_{cr} a^2}{E_m h^3}$$

- The sandwich FG rectangular microplate:

$$\bar{\omega} = \frac{\omega a^2}{h}\sqrt{\frac{\rho_0}{E_0}};\ \bar{\lambda}_{cr} = \frac{\lambda_{cr} a^2}{100h^3 E_0};\ \text{where } E_0 = 1 \text{ GPa and } \rho_0 = 1 \text{ kg/m}^3$$

- The isotropic FG circular microplate:

$$\bar{\lambda}_{cr} = \frac{\lambda_{cr} R^2}{D_m};\ \text{where } D_m = \frac{E_m h^3}{12\left(1-\nu_m^2\right)}$$

**Table 1:** Material properties

| Material properties | Isotropic | Al | Ti | $ZrO_2$ | $ZrO_2$-1 | $Al_2O_3$ |
|---|---|---|---|---|---|---|
| $E$ (GPa) | 1 | 70 | 278.41 | 151 | 200 | 380 |
| $\nu$ | 0.3 | 0.3 | 0.288 | 0.3 | 0.3 | 0.3 |
| $\rho$ (kg/m$^3$) | 1 | 2707 | - | 3000 | 5700 | 3800 |

### *4.1 Static analysis*

#### *4.1.1 Study of convergence*

Let us consider an isotropic simply supported square microplate subjected to a sinusoidally distributed load ( $q_0 = \bar{q}_0 \sin\left(\frac{\pi x}{a}\right)\sin\left(\frac{\pi y}{a}\right)$). The length-to-thickness ratio is taken equal 20 ($a/h$=20). Several values of material length scale-to-thickness ratio ($l/h$=0, 0.2, 0.6, 1) are employed. The square microplate is modeled by 11×11, 17×17, 23×23 and 31×31 nodes as illustrated in Fig. 4. In addition, we consider the influence of the scale factor on the underlying solution. The convergence of the non-dimensional displacement of HSDT meshfree model is given in Tab. 2. The results obtained are compared with those reported by Thai et al. [Thai and Kim (2013)] based on a TSDT analytical model (Anal) and Nguyen et al. [Nguyen, Nguyen, Wahab et al. (2017)] based on a RPT isogeometric analysis (IGA) model. The percentage error (%) of displacement between the present and analytical solutions is given in parenthesis. We see that the present solution converges well to the analytical solution when increasing a number of nodes as well as the scale factor. Also, the increase of the material length scale-to-thickness ratio $l/h$ results in the decrease of the non-dimensional displacement. Hence, the stiffness of isotropic microplate increases when taking into account size-dependent effect. From Tab. 2, it can be seen that the present solution is in very good agreement with the reference solution at the value $\alpha = 2.6$. Therefore, this scale factor value can be used for other next examples.

**Table 2:** Convergence of non-dimensional central displacement $\bar{w}$ of simply supported isotropic square microplate subjected to sinusoidally distributed load

| *l/h* | $\alpha$ | Number of nodes | | | | IGA-RPT | Anal-TSDT |
|---|---|---|---|---|---|---|---|
| | | 11×11 | 17×17 | 23×23 | 31×31 | | |
| 0 | | | | | | 0.2842 | 0.2842 |
| | 2.4 | 0.2792 | 0.2823 | 0.2833 | 0.2838 | | |
| | 2.6 | 0.2798 | 0.2829 | 0.2836 | 0.2840 | | |
| | 2.8 | 0.2841 | 0.2844 | 0.2844 | 0.2844 | | |
| | 3.0 | 0.2858 | 0.2850 | 0.2847 | 0.2845 | | |
| 0.2 | | | | | | 0.2431 | 0.2430 |
| | 2.4 | 0.2384 | 0.2413 | 0.2422 | 0.2426 | | |
| | 2.6 | 0.2388 | 0.2417 | 0.2424 | 0.2428 | | |
| | 2.8 | 0.2424 | 0.2430 | 0.2430 | 0.2430 | | |
| | 3.0 | 0.2439 | 0.2435 | 0.2433 | 0.2432 | | |
| 0.6 | | | | | | 0.1127 | 0.1124 |
| | 2.4 | 0.1100 | 0.1116 | 0.1121 | 0.1123 | | |
| | 2.6 | 0.1099 | 0.1117 | 0.1121 | 0.1123 | | |
| | 2.8 | 0.1113 | 0.1122 | 0.1123 | 0.1124 | | |
| | 3.0 | 0.1123 | 0.1125 | 0.1125 | 0.1125 | | |
| 1.0 | | | | | | 0.0544 | 0.0542 |
| | 2.4 | 0.0530 | 0.0538 | 0.0540 | 0.0541 | | |
| | 2.6 | 0.0529 | 0.0538 | 0.0540 | 0.0541 | | |
| | 2.8 | 0.0535 | 0.0540 | 0.0541 | 0.0542 | | |
| | 3.0 | 0.0540 | 0.0542 | 0.0542 | 0.0542 | | |

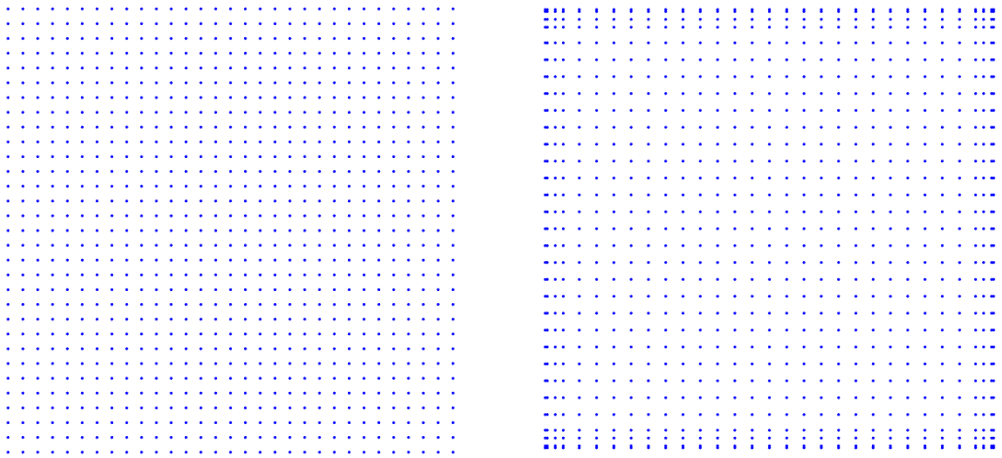

(a) (b)

**Figure 4:** A distributed nodes: (a) Simply supported BCs; (b) Fully clamped BCs

*4.1.2 Accuracy of present solution*

A FG square microplate made of a mixture of ceramic ($Al_2O_3$) and metal (Al) is subjected to a sinusoidally distributed transverse load. Two types of simply supported and fully clamped BCs are used.

**Table 3:** Non-dimensional displacement $\bar{w}$ of the $Al/Al_2O_3$ square microplate subjected to sinusoidally distributed load

| *a*/*h* | *n* | Method | *l*/*h* | | | | | |
|---|---|---|---|---|---|---|---|---|
| | | | 0 | 0.2 | 0.4 | 0.6 | 0.8 | 1.0 |
| Simply supported | | | | | | | | |
| | | IGA-RPT | 0.3433 | 0.2898 | 0.1975 | 0.1292 | 0.0871 | 0.0614 |
| | 0 | Anal-TSDT | 0.3433 | 0.2875 | 0.1934 | 0.1251 | 0.0838 | 0.0588 |
| | | Present | 0.3432 | 0.2873 | 0.1932 | 0.1250 | 0.0836 | 0.0587 |
| | | IGA-RPT | 0.6688 | 0.5505 | 0.3601 | 0.2288 | 0.1517 | 0.1060 |
| 5 | 1 | Anal-TSDT | 0.6688 | 0.5468 | 0.3535 | 0.2224 | 0.1464 | 0.1017 |
| | | Present | 0.6686 | 0.5463 | 0.3530 | 0.2221 | 0.1462 | 0.1016 |
| | | IGA-RPT | 1.2271 | 1.0400 | 0.7140 | 0.4694 | 0.3174 | 0.2242 |
| | 10 | Anal-TSDT | 1.2276 | 1.0247 | 0.6908 | 0.4514 | 0.3052 | 0.2158 |
| | | Present | 1.2272 | 1.0236 | 0.6900 | 0.4507 | 0.3047 | 0.2154 |
| | | IGA-RPT | 0.2842 | 0.2431 | 0.1695 | 0.1127 | 0.0767 | 0.0544 |
| | 0 | Anal-TSDT | 0.2842 | 0.2430 | 0.1693 | 0.1124 | 0.0765 | 0.0542 |
| | | Present | 0.2840 | 0.2428 | 0.1691 | 0.1123 | 0.0764 | 0.0541 |
| | | IGA-RPT | 0.5689 | 0.4739 | 0.3157 | 0.2029 | 0.1352 | 0.0947 |
| 20 | 1 | Anal-TSDT | 0.5689 | 0.4737 | 0.3153 | 0.2025 | 0.1349 | 0.0944 |
| | | Present | 0.5685 | 0.4732 | 0.3149 | 0.2022 | 0.1347 | 0.0943 |
| | | IGA-RPT | 0.9537 | 0.8313 | 0.6001 | 0.4102 | 0.2842 | 0.2038 |
| | 10 | Anal-TSDT | 0.9538 | 0.8303 | 0.5986 | 0.4090 | 0.2834 | 0.2033 |
| | | Present | 0.9532 | 0.8297 | 0.5980 | 0.4085 | 0.2831 | 0.2030 |
| | | IGA-RPT | 0.2804 | 0.2401 | 0.1677 | 0.1116 | 0.0760 | 0.0539 |
| | 0 | Anal-TSDT | 0.2804 | 0.2401 | 0.1677 | 0.1116 | 0.0760 | 0.0539 |
| | | Present | 0.2800 | 0.2397 | 0.1674 | 0.1114 | 0.0759 | 0.0538 |
| | | IGA-RPT | 0.5625 | 0.4689 | 0.3128 | 0.2012 | 0.1341 | 0.0939 |
| 100 | 1 | Anal-TSDT | 0.5625 | 0.4689 | 0.3128 | 0.2011 | 0.1341 | 0.0939 |
| | | Present | 0.5616 | 0.4681 | 0.3122 | 0.2008 | 0.1339 | 0.0937 |
| | | IGA-RPT | 0.9362 | 0.8176 | 0.5925 | 0.4062 | 0.2820 | 0.2024 |
| | 10 | Anal-TSDT | 0.9362 | 0.8176 | 0.5925 | 0.4061 | 0.2820 | 0.2024 |
| | | Present | 0.9348 | 0.8163 | 0.5914 | 0.4054 | 0.2814 | 0.2020 |

| | | | | | | | | |
|---|---|---|---|---|---|---|---|---|
| Fully clamped | | | | | | | | |
| | | IGA-RPT | 0.1601 | 0.1378 | 0.0974 | 0.0655 | 0.0450 | 0.0321 |
| | 0 | IGA-HSDT | 0.1642 | 0.1322 | 0.0840 | 0.0524 | 0.0343 | 0.0238 |
| | | Present | 0.1616 | 0.1300 | 0.0825 | 0.0516 | 0.0339 | 0.0226 |
| | | IGA-RPT | 0.3021 | 0.2555 | 0.1751 | 0.1151 | 0.0779 | 0.0551 |
| 5 | 1 | IGA-HSDT | 0.3097 | 0.2441 | 0.1501 | 0.0916 | 0.0593 | 0.0408 |
| | | Present | 0.3061 | 0.2387 | 0.1473 | 0.0908 | 0.0581 | 0.0395 |
| | | IGA-RPT | 0.6111 | 0.5178 | 0.3568 | 0.2358 | 0.1602 | 0.1136 |
| | 10 | IGA-HSDT | 0.6264 | 0.4908 | 0.3025 | 0.1866 | 0.1221 | 0.0847 |
| | | Present | 0.6162 | 0.4813 | 0.2971 | 0.1829 | 0.1220 | 0.0826 |
| | | IGA-RPT | 0.1035 | 0.0919 | 0.0688 | 0.0485 | 0.0343 | 0.0250 |
| | 0 | IGA-HSDT | 0.1042 | 0.0888 | 0.0615 | 0.0407 | 0.0276 | 0.0195 |
| | | Present | 0.1037 | 0.0882 | 0.0610 | 0.0403 | 0.0273 | 0.0194 |
| | | IGA-RPT | 0.2065 | 0.1797 | 0.1294 | 0.0882 | 0.0611 | 0.0438 |
| 20 | 1 | IGA-HSDT | 0.2077 | 0.1724 | 0.1142 | 0.0731 | 0.0486 | 0.0340 |
| | | Present | 0.2060 | 0.1708 | 0.1131 | 0.0724 | 0.0482 | 0.0337 |
| | | IGA-RPT | 0.3505 | 0.3150 | 0.2419 | 0.1746 | 0.1258 | 0.0926 |
| | 10 | IGA-HSDT | 0.3535 | 0.3056 | 0.2179 | 0.1478 | 0.1020 | 0.0730 |
| | | Present | 0.3513 | 0.3030 | 0.2156 | 0.1461 | 0.1008 | 0.0721 |
| | | IGA-RPT | 0.0999 | 0.0889 | 0.0668 | 0.0473 | 0.0336 | 0.0244 |
| | 0 | IGA-HSDT | 0.0999 | 0.0855 | 0.0597 | 0.0397 | 0.0271 | 0.0192 |
| | | Present | 0.0976 | 0.0836 | 0.0584 | 0.0389 | 0.0265 | 0.0188 |
| | | IGA-RPT | 0.2003 | 0.1746 | 0.1262 | 0.0863 | 0.0599 | 0.0430 |
| 100 | 1 | IGA-HSDT | 0.2004 | 0.1670 | 0.1114 | 0.0716 | 0.0478 | 0.0334 |
| | | Present | 0.1956 | 0.1631 | 0.1088 | 0.0700 | 0.0467 | 0.0327 |
| | | IGA-RPT | 0.3336 | 0.3013 | 0.2336 | 0.1701 | 0.1232 | 0.0910 |
| | 10 | IGA-HSDT | 0.3337 | 0.2914 | 0.2111 | 0.1446 | 0.1004 | 0.0721 |
| | | Present | 0.3264 | 0.2849 | 0.2062 | 0.1413 | 0.0981 | 0.0704 |

Tab. 3 shows the non-dimensional central displacement of isotropic FG square microplates for several values of power index ($n$) and length-to-thickness ratio ($a/h$) as well as material length scale-to-thickness ratio ($l/h$). Reference solutions reported by Thai et al. [Thai and Kim (2013)] using the TSDT analytical model (5 degrees of freedom (DOFs)), Nguyen et al. [Nguyen, Nguyen, Wahab et al. (2017)] using the IGA-RPT model (4 DOFs) and the present HSDT model using IGA are also listed. We observe that obtained results almost match with the reference ones. Basically, the non-dimensional displacements derived from the IGA-RPT model are larger than those of the exact-TSDT model due to using two different theory models. The results of the present model are

mostly close to the published ones in Thai et al. [Thai and Kim (2013)] than those studied by Nguyen et al. [Nguyen, Nguyen, Wahab et al. (2017)] due to using the same TSDT instead of RPT. Also,

Tab. 3 shows that an increase of *l/h* results in a decline of the non-dimensional displacement. The stiffness of FG microplate increases when considering the size-dependent effect. When the power index *n* is increased, the non-dimensional displacement is increased due to decreasing the stiffness of FG microplate. Reciprocally, the length-to-thickness ratio *a/h* risen leads to a reduction of the non-dimensional displacement. For the case of *l/h*=1, the non-dimensional displacement predicted by the size-dependent model is much smaller than about five times those predicted by the classical plate model.

### *4.2 Free vibration and buckling analyses*

#### *4.2.1 Isotropic FG square microplate*

A simply supported isotropic $Al/Al_2O_3$ FG square microplate as given in Subsection 4.1.2 is used for free vibration analysis, while, for buckling analysis, material properties are taken by Reddy [Reddy (2000)]: $E_c = 14.4$ GPa , $E_m = 1.44$ GPa and $\nu_c = \nu_m = 0.38$. Tab. 4 lists the first non-dimensional natural frequency. For comparison, the results reported by Thai et al. [Thai and Kim (2013)] and Nguyen et al. [Nguyen, Nguyen, Wahab et al. (2017)] is also provided in Tab. 4. Also, the non-dimensional critical buckling load obtained by the present meshfree solution based on HSDT, the analytical solution based on FSDT [Thai and Choi (2013)], the analytical solution based on RPT [He, Lou, Zhang et al. (2015)] and the IGA solution based on RPT [Nguyen, Nguyen, Wahab et al. (2017)] is given in Tab. 5. As observed from Tab. 4 and Tab. 5, a good agreement with those reference results is achieved. Basically, the results of the present model are slightly larger than compared to those of the above reference solutions for both non-dimensional natural frequency and critical buckling load. Especially, obtained results are mostly close to the published solution by Thai et al. [Thai and Kim (2013)] than that of other published results because of using the same HSDT model. Moreover, according to two above tables, it can be observed that $\bar{\omega}$ and $\bar{\lambda}_{cr}$ increase as *l/h* increases. The vibration and buckling responses predicted by the MCST are always larger than those of the classical theory. The non-dimensional natural frequency and critical buckling load given by the classical plate model are much smaller than two and five times those given by the size-dependent model with *l*/*h*=1, respectively. These differences decrease when the plate thickness of becomes large. We can conclude that the stiffness of FG microplate increases with respect to inclusion of the size effect leading to a rise of natural frequency as well as critical buckling load.

**Table 4:** The first non-dimensional natural frequency $\bar{\omega}$ of simply supported FG square microplate

| *a*/*h* | *n* | Method | *l*/*h* | | | | | |
|---|---|---|---|---|---|---|---|---|
| | | | 0 | 0.2 | 0.4 | 0.6 | 0.8 | 1.0 |
| 5 | 0 | Anal-TSDT | 5.2813 | 5.7699 | 7.0330 | 8.7389 | 10.6766 | 12.7408 |
| | | IGA-RPT | 5.2813 | 5.7496 | 6.9667 | 8.6191 | 9.8943 | 9.9791 |
| | | Present | 5.2832 | 5.7742 | 7.0412 | 8.7510 | 10.6926 | 12.7606 |
| | 1 | Anal-TSDT | 4.0781 | 4.5094 | 5.6071 | 7.0662 | 8.7058 | 10.4397 |
| | | IGA-RPT | 4.0781 | 4.4959 | 5.5620 | 6.9822 | 8.2313 | 8.3019 |
| | | Present | 4.0780 | 4.5113 | 5.6117 | 7.0735 | 8.7156 | 10.4519 |
| | 10 | Anal-TSDT | 3.2514 | 3.5548 | 4.3200 | 5.3335 | 6.4759 | 7.6895 |
| | | IGA-RPT | 3.2519 | 3.5312 | 4.2584 | 5.2471 | 5.8571 | 5.9073 |
| | | Present | 3.2501 | 3.5577 | 4.3251 | 5.3409 | 6.4857 | 7.7018 |
| 20 | 0 | Anal-TSDT | 5.9199 | 6.4027 | 7.6708 | 9.4116 | 11.4108 | 13.5545 |
| | | IGA-RPT | 5.9199 | 6.4009 | 7.6646 | 9.4005 | 11.3945 | 13.5330 |
| | | Present | 5.9250 | 6.4091 | 7.6801 | 9.4244 | 11.4272 | 13.5746 |
| | 1 | Anal-TSDT | 4.5228 | 4.9568 | 6.0756 | 7.5817 | 9.2887 | 11.1042 |
| | | IGA-RPT | 4.5228 | 4.9556 | 6.0714 | 7.5739 | 9.2768 | 11.0882 |
| | | Present | 4.5270 | 4.9621 | 6.0835 | 7.5926 | 9.3026 | 11.1212 |
| | 10 | Anal-TSDT | 3.7622 | 4.0323 | 4.7488 | 5.7453 | 6.9013 | 8.1494 |
| | | IGA-RPT | 3.7623 | 4.0299 | 4.7428 | 5.7369 | 6.8914 | 8.1384 |
| | | Present | 3.7651 | 4.0360 | 4.7546 | 5.7534 | 6.9119 | 8.1625 |

**Table 5:** Comparison of non-dimensional critical buckling load $\bar{\lambda}_{cr}$ of simply supported FG square microplates

| *a*/*h* | *n* | Method | *l*/*h* | | | | | |
|---|---|---|---|---|---|---|---|---|
| | | | 0 | 0.2 | 0.4 | 0.6 | 0.8 | 1.0 |
| 5 | 0 | Anal-FSDT | 15.3228 | 17.6150 | 24.2899 | 34.7856 | 48.2915 | 63.8913 |
| | | Anal-RPT | 15.3322 | 18.0422 | 26.1539 | 39.6393 | 58.4862 | 82.6938 |
| | | IGA-RPT | 15.3321 | 17.8878 | 25.5457 | 38.2867 | 56.0961 | 78.9675 |
| | | Present | 15.3498 | 18.0767 | 26.2253 | 39.7655 | 58.6858 | 82.9864 |
| | 1 | Anal-FSDT | 6.8576 | 8.1715 | 11.9922 | 17.9838 | 25.6654 | 34.4981 |
| | | Anal-RPT | 6.8611 | 8.3399 | 12.7754 | 20.1658 | 30.5105 | 43.8094 |
| | | IGA-RPT | 6.8610 | 8.2820 | 12.5322 | 19.5858 | 29.4240 | 42.0388 |
| | | Present | 6.8693 | 8.3572 | 12.8126 | 20.2329 | 30.6177 | 43.9673 |
| | 10 | Anal-FSDT | 2.9979 | 3.4076 | 4.6013 | 6.4804 | 8.9020 | 11.7042 |
| | | Anal-RPT | 2.7672 | 3.3619 | 5.0407 | 7.7001 | 11.3322 | 15.9522 |
| | | IGA-RPT | 2.7702 | 3.2917 | 4.8371 | 7.3772 | 10.9005 | 15.4071 |
| | | Present | 2.7708 | 3.3691 | 5.0551 | 7.7255 | 11.3729 | 16.0125 |

| | | | | | | | | |
|---|---|---|---|---|---|---|---|---|
| 10 | 0 | Anal-FSDT | 18.0746 | 20.7607 | 28.7478 | 41.8271 | 59.6657 | 81.8269 |
| | | Anal-RPT | 18.0754 | 20.9025 | 29.3735 | 43.4732 | 63.1958 | 88.5416 |
| | | IGA-RPT | 18.0756 | 20.8497 | 29.1700 | 43.0329 | 62.4358 | 87.3775 |
| | | Present | 18.1013 | 20.9405 | 29.4453 | 43.5986 | 63.3946 | 88.8337 |
| | 1 | Anal-FSDT | 7.8273 | 9.3241 | 13.7742 | 21.0597 | 30.9928 | 43.3274 |
| | | Anal-RPT | 7.8276 | 9.3767 | 14.0232 | 21.7657 | 32.6036 | 46.5372 |
| | | IGA-RPT | 7.8277 | 9.3581 | 13.9459 | 21.5846 | 32.2693 | 45.9981 |
| | | Present | 7.8402 | 9.3959 | 14.0608 | 21.8324 | 32.7101 | 46.6940 |
| | 10 | Anal-FSDT | 3.5853 | 4.0710 | 5.5151 | 7.8802 | 11.1065 | 15.1152 |
| | | Anal-RPT | 3.4969 | 4.0513 | 5.6631 | 8.2906 | 11.9349 | 16.6033 |
| | | IGA-RPT | 3.4982 | 4.0246 | 5.5925 | 8.1871 | 11.8036 | 16.4431 |
| | | Present | 3.5015 | 4.0587 | 5.6778 | 8.3167 | 11.9765 | 16.6645 |
| 20 | 0 | Anal-FSDT | 18.9243 | 21.7387 | 30.1625 | 44.1369 | 63.5656 | - |
| | | Anal-RPT | 18.9243 | 21.7771 | 30.3324 | 44.5855 | 64.5348 | 90.1804 |
| | | IGA-RPT | 18.9244 | 21.7628 | 30.2773 | 44.4673 | 64.3321 | 89.8715 |
| | | Present | 18.9661 | 21.8309 | 30.4212 | 44.7308 | 64.7576 | 90.5014 |
| | 1 | Anal-FSDT | 8.1142 | 9.6675 | 14.3167 | 22.0292 | 32.7517 | - |
| | | Anal-RPT | 8.1142 | 9.6815 | 14.3832 | 22.2188 | 33.1882 | 47.2914 |
| | | IGA-RPT | 8.1143 | 9.6766 | 14.3626 | 22.1708 | 33.0999 | 47.1494 |
| | | Present | 8.1336 | 9.7077 | 14.4290 | 22.2959 | 33.3079 | 47.4648 |
| | 10 | Anal-FSDT | 3.7700 | 4.2809 | 5.8102 | 8.3472 | 11.8745 | - |
| | | Anal-RPT | 3.7450 | 4.2752 | 5.8505 | 8.4589 | 12.1011 | 16.7793 |
| | | IGA-RPT | 3.7454 | 4.2677 | 5.8312 | 8.4312 | 12.0666 | 16.7376 |
| | | Present | 3.7525 | 4.2854 | 5.8682 | 8.4886 | 12.1472 | 16.8462 |

*4.2.2 Isotropic FG circular plate*

We consider an isotropic $Ti/ZrO_2$ FG circular microplate with the radius $R$ and the thickness $h$ subjected to a uniform radial compression, as shown in Fig. 5(a). The simply supported and fully clamped boundary conditions are studied and a distribution of nodes is shown in Fig. 5(b-c). In addition, the effective Young's modulus and Poison's ratio are computed by:

$$E_e = (E_m - E_c)V(z) + E_c;\ \ \nu_e = (\nu_m - \nu_c)V(z) + \nu_c;\ V(z) = \left(\frac{1}{2} - \frac{z}{h}\right)^n \tag{49}$$

Again, different values of power index, thickness-to-radius ratio and material length scale-to-thickness ratio are studied. The non-dimensional critical buckling load of the present model is listed in Tab. 6. Obtained results of $l/h$=0 are compared with those reported by Ma et al. [Ma and Wang (2004)] using the analytical solution based on FSDT and TSDT, Saidi et al. [Saidi, Rasouli and Sahraee (2009)] using the analytical solution based on unconstrained third-order shear deformation plate theory (UTSDT) and

Nguyen-Xuan et al. [Nguyen-Xuan, Tran, Thai et al. (2014)] using the IGA based on RPT. The present results match well with the referenced ones for the case of $l/h$=0. In addition, it is noted that the non-dimensional critical buckling load increases when increasing the material length scale-to-thickness ratio. The stiffness of microplate increases within considering size-dependent effects. The difference of critical buckling load between the present size-dependent model ($l/h$=1) and the classical model is most significant but this difference decreases when the thickness of the microplate becomes large. The first six modes shape of buckling response of fully clamped isotropic FG circular microplate is plotted in Fig. 6.

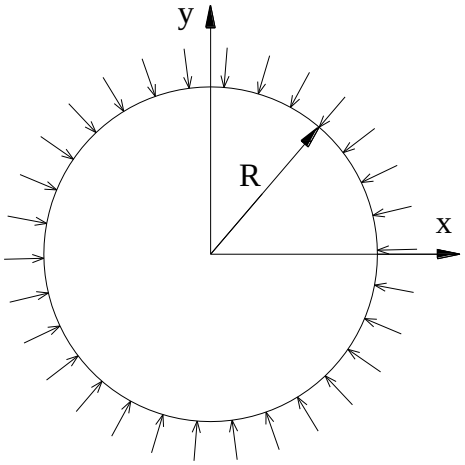


(a)

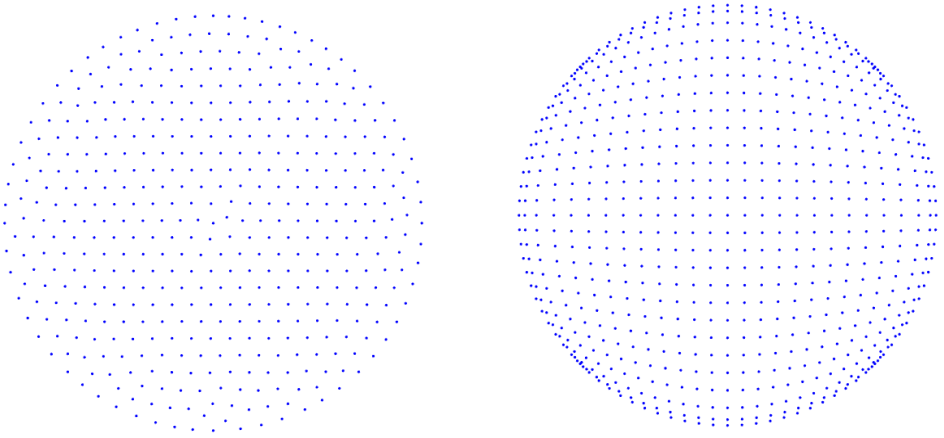

(b) (c)

**Figure 5:** The circular microplate: a) Geometry; b) Distribution nodes for simply supported BC; Distribution nodes for simply clamped BC

**Table 6:** Non-dimensional critical buckling load factor $\bar{\lambda}_{cr}$ of isotropic FG circular microplates

| *n* | *l*/*h* | Method | *h*/*R* | | | |
|---|---|---|---|---|---|---|
| | | | 0.1 | 0.2 | 0.25 | 0.3 |
| Simply supported | | | | | | |
| 0 | 0 | Present | 4.1554 | 4.0113 | 3.9103 | 3.7938 |
| | | Anal-FSDT | 4.1502 | 4.0075 | 3.9071 | 3.7905 |
| | | Anal-TSDT | 4.1502 | 4.0077 | 3.9072 | 3.7911 |
| | | Anal-UTSDT | 4.1503 | 4.0079 | 3.9072 | 3.7911 |
| | 0.2 | Present | 4.2827 | 4.1418 | 4.0436 | 3.9304 |
| | 0.4 | Present | 4.5151 | 4.3720 | 4.2767 | 4.1680 |
| | 0.6 | Present | 4.7078 | 4.5685 | 4.4798 | 4.3797 |
| | 0.8 | Present | 4.8420 | 4.7148 | 4.6357 | 4.5470 |
| | 1.0 | Present | 4.9334 | 4.8216 | 4.7527 | 4.6756 |
| 0.5 | 0 | Present | 5.7265 | 5.5264 | 5.3861 | 5.2244 |
| | | Anal-FSDT | 5.7204 | 5.5249 | 5.3868 | 5.2273 |
| | | Anal-TSDT | 5.7196 | 5.5213 | 5.3819 | 5.2206 |
| | | Anal-UTSDT | 5.7198 | 5.5217 | 5.3819 | 5.2208 |
| | 0.2 | Present | 5.9030 | 5.7080 | 5.5723 | 5.4156 |
| | 0.4 | Present | 6.2246 | 6.0279 | 5.8971 | 5.7477 |
| | 0.6 | Present | 6.4907 | 6.3004 | 6.1793 | 6.0426 |
| | 0.8 | Present | 6.6759 | 6.5027 | 6.3951 | 6.2745 |
| | 1.0 | Present | 6.8017 | 6.6499 | 6.5565 | 6.4519 |
| 2 | 0 | Present | 6.7868 | 6.5734 | 6.4230 | 6.2486 |
| | | Anal-FSDT | 6.7764 | 6.5616 | 6.4088 | 6.2318 |
| | | Anal-TSDT | 6.778 | 6.5671 | 6.4176 | 6.2437 |
| | | Anal-UTSDT | 6.7783 | 6.5672 | 6.4179 | 6.2441 |
| | 0.2 | Present | 7.0085 | 6.7968 | 6.6489 | 6.4777 |
| | 0.4 | Present | 7.4015 | 7.1798 | 7.0327 | 6.8649 |
| | 0.6 | Present | 7.7160 | 7.4968 | 7.3580 | 7.2015 |
| | 0.8 | Present | 7.9298 | 7.7289 | 7.6044 | 7.4649 |
| | 1.0 | Present | 8.0733 | 7.8967 | 7.7881 | 7.6667 |
| 10 | 0 | Present | 7.9835 | 7.7284 | 7.5487 | 7.3405 |
| | | Anal-FSDT | 7.9717 | 7.7149 | 7.5325 | 7.3217 |
| | | Anal-TSDT | 7.9733 | 7.7213 | 7.5424 | 7.3353 |
| | | Anal-UTSDT | 7.9730 | 7.7211 | 7.5425 | 7.3348 |

| | | | | | | |
|---|---|---|---|---|---|---|
| | 0.2 | Present | 8.2409 | 7.9877 | 7.8109 | 7.6064 |
| | 0.4 | Present | 8.6997 | 8.4345 | 8.2585 | 8.0578 |
| | 0.6 | Present | 9.0691 | 8.8065 | 8.6400 | 8.4525 |
| | 0.8 | Present | 9.3215 | 9.0800 | 8.9304 | 8.7629 |
| | 1.0 | Present | 9.4914 | 9.2786 | 9.0017 | 9.1479 |
| Fully clamped | | | | | | |
| | 0 | Present | 14.2065 | 12.5651 | 11.5961 | 10.6109 |
| | | Anal-TSDT | 14.089 | 12.574 | 11.638 | 10.670 |
| | | Anal-UTSDT | 14.089 | 12.575 | 11.639 | 10.670 |
| | | IGA-RPT | 14.2023 | 12.7281 | 11.8143 | 10.8666 |
| 0 | 0.2 | Present | 16.7292 | 15.0790 | 14.0771 | 13.0388 |
| | 0.4 | Present | 24.2239 | 22.3498 | 21.1718 | 19.9246 |
| | 0.6 | Present | 36.6708 | 34.3840 | 32.9086 | 31.3169 |
| | 0.8 | Present | 54.0748 | 51.1961 | 49.3047 | 47.2345 |
| | 1.0 | Present | 76.4396 | 72.7922 | 70.3660 | 67.6829 |
| | 0 | Present | 19.5774 | 17.3032 | 15.9615 | 14.5985 |
| | | Anal-TSDT | 19.411 | 17.311 | 16.013 | 14.672 |
| | | Anal-UTSDT | 19.413 | 17.310 | 16.012 | 14.672 |
| | | IGA-RPT | 19.5663 | 17.5180 | 16.2506 | 14.9381 |
| 0.5 | 0.2 | Present | 23.0780 | 20.7999 | 19.4168 | 17.9839 |
| | 0.4 | Present | 33.4762 | 30.9155 | 29.3037 | 27.5957 |
| | 0.6 | Present | 50.7425 | 47.6515 | 45.6524 | 43.4915 |
| | 0.8 | Present | 78.8827 | 71.0254 | 68.4831 | 65.6935 |
| | 1.0 | Present | 105.9024 | 101.0456 | 97.8042 | 94.2092 |
| | 0 | Present | 23.2864 | 20.8136 | 19.3306 | 17.8035 |
| | | Anal-TSDT | 23.074 | 20.803 | 19.377 | 17.882 |
| | | Anal-UTSDT | 23.075 | 20.805 | 19.378 | 17.881 |
| | | IGA-RPT | 23.2592 | 21.0569 | 19.6687 | 18.2099 |
| 2 | 0.2 | Present | 25.2108 | 25.2108 | 23.6579 | 22.0308 |
| | 0.4 | Present | 40.9735 | 37.9928 | 36.1025 | 34.0859 |
| | 0.6 | Present | 62.9775 | 59.1824 | 56.7222 | 54.0572 |
| | 0.8 | Present | 93.7558 | 88.8070 | 85.5498 | 81.9791 |
| | 1.0 | Present | 133.3138 | 126.8754 | 122.5941 | 117.8601 |
| | 0 | Present | 27.3717 | 24.4195 | 22.6543 | 20.8406 |
| 10 | | Anal-TSDT | 27.133 | 24.423 | 22.725 | 20.948 |
| | | Anal-UTSDT | 27.131 | 24.422 | 22.725 | 20.949 |

| | | | | | |
|---|---|---|---|---|---|
| | IGA-RPT | 27.3429 | 24.6994 | 23.0389 | 21.2986 |
| 0.2 | Present | 32.5238 | 29.5116 | 27.6637 | 25.7317 |
| 0.4 | Present | 47.8534 | 44.2957 | 42.0458 | 39.6513 |
| 0.6 | Present | 73.3303 | 68.7999 | 65.8715 | 62.7064 |
| 0.8 | Present | 108.9654 | 103.0579 | 99.1801 | 94.9385 |
| 1.0 | Present | 154.7654 | 147.0802 | 141.9824 | 136.3578 |

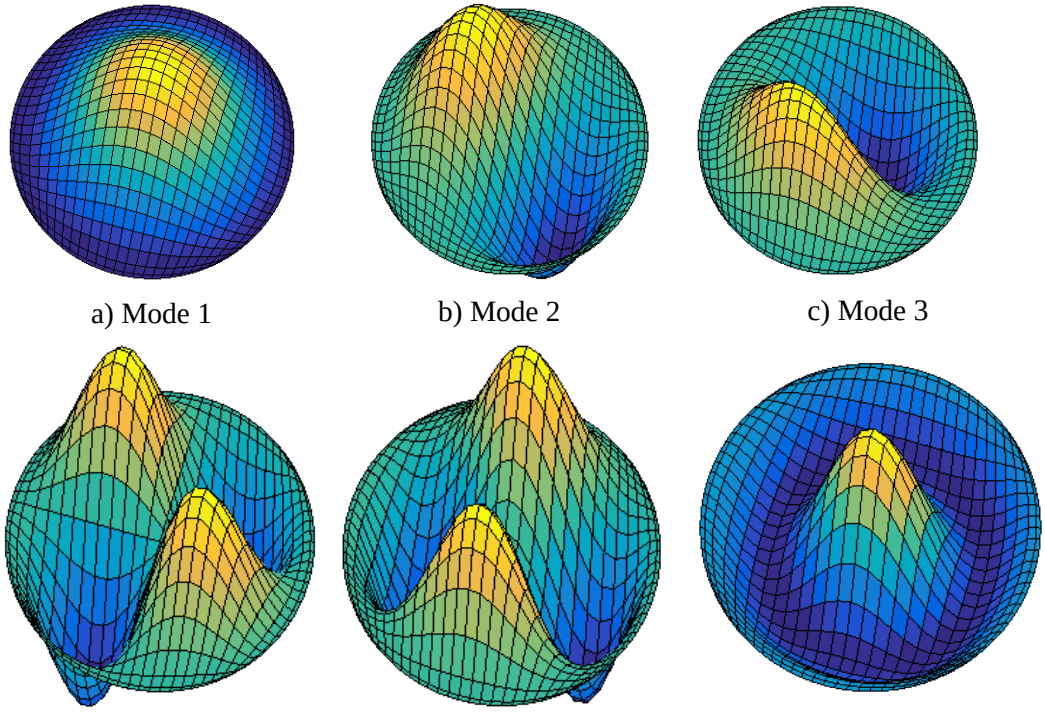

a) Mode 1 b) Mode 2 c) Mode 3

d) Mode 4 e) Mode 5 f) Mode 6

**Figure 6:** The first six mode shapes of buckling response of fully clamped isotropic FG circular microplate with n=10, h/R=0.1 and l/h=1

*4.2.3 Isotropic FG square plate with a complicated cutout*

We consider a simply supported square microplate with a complicated cutout, as shown in Fig. 7(a). A set of nodes (541 nodes) of the isotropic FG microplate is illustrated by Fig. 7(b). This microplate is made of zirconia ($ZrO_2$-2) and aluminum (Al). The non-dimensional natural frequency is given by $\bar{\omega} = \omega \frac{a^2}{h} \sqrt{\rho_c / E_c}$, where $E_c$ and $\rho_c$ are the Young's modulus and density mass of ceramic, respectively. The first six non-dimensional natural frequencies of the square FG microplate with a complicated cutout are given in Tab. 7. For the case of $l/h = 0$, obtained results are compared with those

reported in Nguyen et al. [Nguyen and Nguyen-Xuan (2015)] based on the IGA solution using 3D elasticity theory (IGA-3D) and in [Thai, Ferreira, Wahab et al. (2018)] based on the meshfree solution using HSDT (MF-HSDT). In addition, the present results are available for the case of $l/h \neq 0$. As given in Tab. 7, non-dimensional frequencies increase with increasing of $l/h$ and decrease when increasing the power index value.

**Table 7:** Comparisons of non-dimensional frequencies $\bar{\omega}$ of the isotropic FG square plate of a hole of complicated shape

| *n* | *l/h* | Method | Modes | | | | | |
|---|---|---|---|---|---|---|---|---|
| | | | 1 | 2 | 3 | 4 | 5 | 6 |
| 0 | 0 | Present | 7.1633 | 11.7279 | 13.2402 | 21.1831 | 21.8449 | 22.8302 |
| | | IGA-3D | 7.16 | 11.65 | 13.09 | 20.99 | 21.85 | 22.54 |
| | | MF-HSDT | 7.1586 | 11.9392 | 13.3987 | 21.5109 | 22.4376 | 23.4263 |
| | 0.2 | Present | 9.4917 | 15.7649 | 17.5282 | 21.9521 | 26.7706 | 29.7840 |
| | 0.4 | Present | 13.9456 | 22.2547 | 23.3754 | 25.7099 | 37.5234 | 38.9547 |
| | 0.6 | Present | 18.9899 | 22.7211 | 31.9503 | 35.0228 | 39.5221 | 40.4706 |
| | 0.8 | Present | 23.3244 | 24.2884 | 40.1927 | 40.9425 | 41.1735 | 44.8261 |
| | 1.0 | Present | 24.0422 | 29.7200 | 40.9153 | 41.9082 | 50.1524 | 54.8809 |
| 1 | 0 | Present | 6.5901 | 10.8096 | 12.1998 | 19.5276 | 20.8860 | 21.0809 |
| | | IGA-3D | 6.58 | 10.73 | 12.06 | 19.35 | 20.77 | 20.92 |
| | | MF-HSDT | 6.5853 | 11.0022 | 12.3439 | 19.8282 | 21.4529 | 21.6277 |
| | 0.2 | Present | 8.8771 | 14.7652 | 16.4046 | 21.0001 | 24.9995 | 27.8714 |
| | 0.4 | Present | 13.1889 | 21.2790 | 22.1233 | 24.3231 | 35.4222 | 37.2534 |
| | 0.6 | Present | 18.0472 | 21.7005 | 30.3759 | 33.2915 | 37.7699 | 38.6757 |
| | 0.8 | Present | 22.2419 | 23.1387 | 38.3759 | 38.9983 | 39.3292 | 42.7120 |
| | 1.0 | Present | 22.8855 | 28.3512 | 39.0341 | 39.9861 | 47.8466 | 52.3578 |
| 5 | 0 | Present | 6.7149 | 10.9500 | 12.3704 | 19.7168 | 19.7683 | 21.2633 |
| | | IGA-3D | 6.71 | 10.88 | 12.24 | 19.60 | 19.73 | 21.00 |
| | | MF-HSDT | 6.7111 | 11.1480 | 12.5192 | 20.0718 | 20.2528 | 21.8177 |
| | 0.2 | Present | 8.7660 | 14.5352 | 16.1717 | 19.8147 | 24.7419 | 27.4735 |
| | 0.4 | Present | 12.7462 | 20.0772 | 21.3673 | 23.5083 | 34.3845 | 35.1503 |
| | 0.6 | Present | 17.2763 | 20.4747 | 29.0887 | 31.8876 | 35.6384 | 36.4924 |
| | 0.8 | Present | 20.9864 | 22.0438 | 36.2091 | 37.0373 | 37.2564 | 40.7271 |
| | 1.0 | Present | 21.5953 | 26.9366 | 36.8322 | 37.7299 | 45.5101 | 49.7974 |
| 20 | 0 | Present | 6.5628 | 10.7100 | 12.0976 | 19.0687 | 19.3370 | 20.8050 |
| | | IGA-3D | 6.46 | 10.48 | 11.79 | 18.89 | 19.05 | 20.25 |
| | | MF-HSDT | 6.5590 | 10.9040 | 12.2431 | 19.5863 | 19.6350 | 21.3484 |
| | 0.2 | Present | 8.5315 | 14.1468 | 15.7422 | 19.1626 | 24.1022 | 26.7535 |
| | 0.4 | Present | 12.3659 | 19.4247 | 20.7245 | 22.8042 | 33.3755 | 34.0025 |
| | 0.6 | Present | 16.7367 | 19.8274 | 28.1721 | 30.8854 | 34.4934 | 35.3210 |
| | 0.8 | Present | 20.3479 | 21.3398 | 35.0721 | 35.9047 | 36.0228 | 39.4146 |
| | 1.0 | Present | 20.9670 | 26.0659 | 35.6974 | 36.5644 | 44.0260 | 48.1750 |

| | | | | | | | | |
|---|---|---|---|---|---|---|---|---|
| 50 | 0 | Present | 6.3681 | 10.4101 | 11.7554 | 18.7994 | 18.8879 | 20.2446 |
| | | IGA-3D | 6.19 | 10.07 | 11.32 | 18.15 | 18.81 | 19.48 |
| | | MF-HSDT | 6.3642 | 10.5978 | 11.8961 | 19.0892 | 19.4004 | 20.7723 |
| | 0.2 | Present | 8.3449 | 13.8489 | 15.4050 | 18.9807 | 23.5627 | 26.1820 |
| | 0.4 | Present | 12.1655 | 19.2418 | 20.3902 | 22.4321 | 32.7917 | 33.6813 |
| | 0.6 | Present | 16.5084 | 19.6442 | 27.7822 | 30.4563 | 34.1710 | 34.9910 |
| | 0.8 | Present | 20.1645 | 21.0772 | 34.7494 | 35.5359 | 35.6054 | 38.9159 |
| | 1.0 | Present | 20.7835 | 25.7650 | 35.3730 | 36.2315 | 43.4999 | 47.6003 |
| 100 | 0 | Present | 6.2704 | 10.2578 | 11.5821 | 18.5260 | 18.8221 | 19.9581 |
| | | IGA-3D | 6.15 | 10.00 | 11.25 | 18.04 | 18.78 | 19.36 |
| | | MF-HSDT | 6.2664 | 10.4427 | 11.7206 | 18.8120 | 19.3328 | 20.4784 |
| | 0.2 | Present | 8.2559 | 13.7065 | 15.2435 | 18.9145 | 23.3010 | 25.9058 |
| | 0.4 | Present | 12.0763 | 19.1751 | 20.2414 | 22.2660 | 32.5265 | 33.5643 |
| | 0.6 | Present | 16.4121 | 19.5767 | 27.6171 | 30.2743 | 34.0529 | 34.8702 |
| | 0.8 | Present | 20.0962 | 20.9704 | 34.6303 | 35.3563 | 35.4765 | 38.7116 |
| | 1.0 | Present | 20.7142 | 25.6456 | 35.2526 | 36.1081 | 43.2889 | 47.3699 |

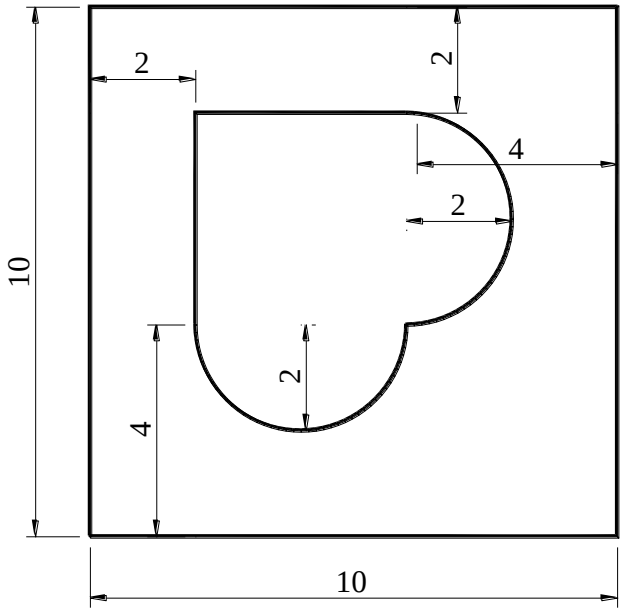


(a)

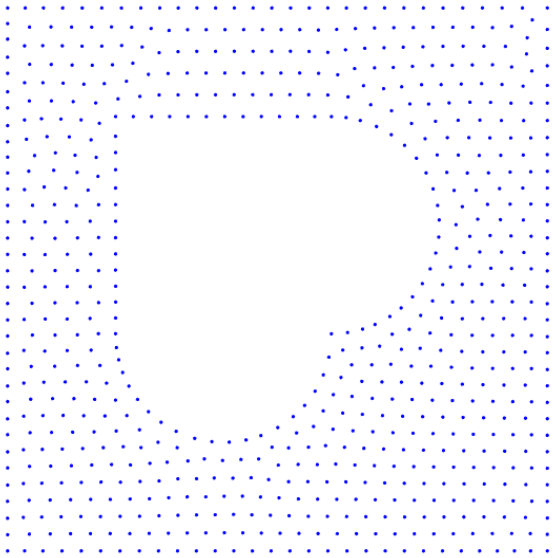

(b)

**Figure 7:** Geometry and a set of distributed node of a square plate with a complicated hole

### *4.2.4 FGM sandwich square plate*

This final example is a simply supported sandwich FG square microplate making from $Al/Al_2O_3$. To evaluate the natural frequency and critical buckling load of sandwich FG square microplate, six types of the bottom-core-top thickness ratio consisting of $h_b - h_c - h_t$ = 1-0-1, 2-1-2, 2-1-1, 1-1-1, 2-2-1, 1-2-1 and various values of the power index as well as material length scale-to-thickness ratio are studied. As known, the solutions using MCST for free vibration and buckling analyses of sandwich FG square microplates are not available in the literature. Therefore, present results are only compared with other referenced ones without considering the size effects. For comparison with $l/h$=0, the non-dimensional natural frequency given by Li et al. [Li, Lu and Kou (2008)] using the analytical solution (Anal) based on 3D elasticity theory, Zenkour [Zenkour (2005)] using the analytical solution based on TSDT and SSDT and Thai et al. [Thai, Kulasegaram, Tran et al. (2014)] using IGA based on TSDT are also provided in Tab. 8, while the bi-axial critical buckling load reported by Reddy [Reddy (2000)] based on the Anal-TSDT solution, Zenkour [Zenkour (2005)] based on the Anal-SSDT solution, Neves et al. [Neves, Ferreira, Carrera et al. (2013)] based on the meshfree-HSDT solution (MF-HSDT) and Thai et al. [Thai, Kulasegaram, Tran et al. (2014] based on IGA-TSDT are given in Tab. 9. According to Tab. 8 and Tab. 9, it is again seen that a rise of the non-dimensional natural frequency and bi-axial critical buckling load is found when increasing the material length scale-to-thickness ratio. Also, the stiffness of sandwich FG microplate increases within considering size effects. In particular, most of non-dimensional natural frequency and critical buckling load with

respect to six types of the bottom-core-top thickness ratio predicted by the present size-dependent MKI-HSDT model are much larger than two and five times those predicted by the classical MKI-HSDT model, respectively. In addition, a change of the bottom-core-top thickness ratio from $1-0-1$ to $1-2-1$ also brings to an increase of the non-dimensional natural frequency as well as critical buckling load. Moreover, Tab. 10 shows the first five non-dimensional natural frequencies and mode shapes of sandwich FG square microplate corresponding with $h_b - h_c - h_t$ = 2-1-2. Besides, the first six mode shapes of sandwich FG square microplate are plotted in Fig. 8.

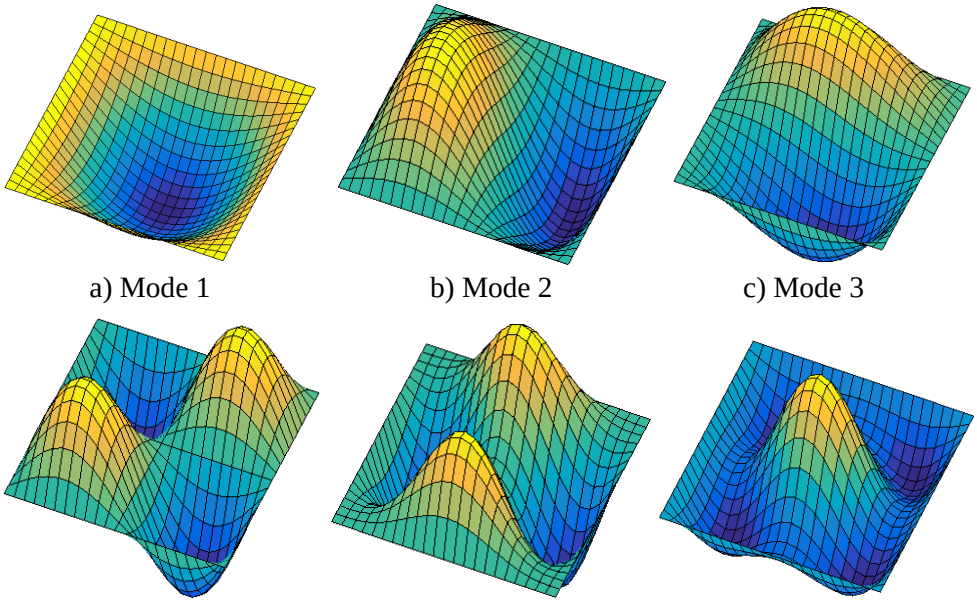

a) Mode 1 b) Mode 2 c) Mode 3

d) Mode 4 e) Mode 5 f) Mode 6

**Figure 8:** The first six modes shape of dynamic response of simply supported sandwich FG square microplate with $n$=1, $l/h$=1 and $h_b - h_c - h_t = 2$ ? ?

**Table 8:** The natural frequency $\bar{\omega}$ of the simply supported sandwich FG microplate with $a/h$=10

| $n$ | $l/h$ | Method | 1-0-1 | 2-1-2 | 2-1-1 | 1-1-1 | 2-2-1 | 1-2-1 |
|---|---|---|---|---|---|---|---|---|
| 0.5 | 0 | Present | 1.4451 | 1.4849 | 1.5073 | 1.5201 | 1.5480 | 1.5754 |
| | | Anal-3D | 1.4461 | 1.4861 | 1.5084 | 1.5213 | 1.5493 | 1.5766 |
| | | Anal-TSDT | 1.4442 | 1.4841 | 1.5125 | 1.5192 | 1.5520 | 1.5745 |
| | | Anal-SSDT | 1.4443 | 1.4842 | 1.5126 | 1.5193 | 1.5520 | 1.5745 |
| | | IGA-TSDT | 1.4443 | 1.4841 | 1.5064 | 1.5192 | 1.5472 | 1.5745 |
| | 0.2 | Present | 1.5984 | 1.6420 | 1.6640 | 1.6785 | 1.7062 | 1.7343 |
| | 0.4 | Present | 1.9883 | 2.0415 | 2.0638 | 2.0825 | 2.1105 | 2.1414 |
| | 0.6 | Present | 2.5065 | 2.5728 | 2.5965 | 2.6206 | 2.6505 | 2.6858 |
| | 0.8 | Present | 3.0888 | 3.1700 | 3.1962 | 3.2263 | 3.2594 | 3.3004 |
| | 1.0 | Present | 3.7052 | 3.8022 | 3.8316 | 3.8679 | 3.9050 | 3.9524 |

| | | | | | | | | |
|---|---|---|---|---|---|---|---|---|
| 1 | 0 | Present | 1.2440 | 1.3009 | 1.3342 | 1.3542 | 1.3965 | 1.4402 |
| | | Anal-3D | 1.2447 | 1.3018 | 1.3351 | 1.3552 | 1.3976 | 1.4413 |
| | | Anal-TSDT | 1.2432 | 1.3001 | 1.3489 | 1.3533 | 1.4079 | 1.4393 |
| | | Anal-SSDT | 1.2433 | 1.3002 | 1.3489 | 1.3534 | 1.4079 | 1.4393 |
| | | IGA-TSDT | 1.2432 | 1.3001 | 1.3334 | 1.3533 | 1.3957 | 1.4393 |
| | 0.2 | Present | 1.3957 | 1.4606 | 1.4936 | 1.5166 | 1.5585 | 1.6034 |
| | 0.4 | Present | 1.7742 | 1.8585 | 1.8923 | 1.9228 | 1.9655 | 2.0147 |
| | 0.6 | Present | 2.2677 | 2.3769 | 2.4138 | 2.4537 | 2.5001 | 2.5566 |
| | 0.8 | Present | 2.8159 | 2.9525 | 2.9942 | 3.0442 | 3.0964 | 3.1623 |
| | 1.0 | Present | 3.3923 | 3.5575 | 3.6051 | 3.6657 | 3.7249 | 3.8014 |
| 5 | 0 | Present | 0.9466 | 0.9826 | 1.0313 | 1.0454 | 1.1098 | 1.1748 |
| | | Anal-3D | 0.9448 | 0.9810 | 1.0294 | 1.0453 | 1.1098 | 1.1757 |
| | | Anal-TSDT | 0.9460 | 0.9818 | 1.0743 | 1.0447 | 1.1473 | 1.1740 |
| | | Anal-SSDT | 0.9463 | 0.9820 | 1.0744 | 1.0448 | 1.1474 | 1.1740 |
| | | IGA-TSDT | 0.9460 | 0.9818 | 1.0306 | 1.0447 | 1.1090 | 1.1740 |
| | 0.2 | Present | 1.0678 | 1.1373 | 1.1877 | 1.2129 | 1.2779 | 1.3473 |
| | 0.4 | Present | 1.3678 | 1.5079 | 1.5647 | 1.6129 | 1.6834 | 1.7654 |
| | 0.6 | Present | 1.7564 | 1.9745 | 2.0420 | 2.1154 | 2.1968 | 2.2969 |
| | 0.8 | Present | 2.1863 | 2.4821 | 2.5632 | 2.6613 | 2.7575 | 2.8784 |
| | 1.0 | Present | 2.6371 | 3.0094 | 3.1060 | 3.2280 | 3.3412 | 3.4845 |
| 10 | 0 | Present | 0.9290 | 0.9437 | 0.9928 | 0.9963 | 1.0618 | 1.1239 |
| | | Anal-3D | 0.9273 | 0.9418 | 0.9893 | 0.9952 | 1.0610 | 1.1247 |
| | | Anal-TSDT | 0.9284 | 0.9430 | 1.0386 | 0.9955 | 1.1053 | 1.1231 |
| | | Anal-SSDT | 0.9288 | 0.9433 | 1.0455 | 0.9952 | 1.0415 | 1.1346 |
| | | IGA-TSDT | 0.9288 | 0.9433 | 0.9923 | 0.9957 | 1.0612 | 1.1232 |
| | 0.2 | Present | 1.0323 | 1.0906 | 1.1429 | 1.1613 | 1.2288 | 1.2975 |
| | 0.4 | Present | 1.2934 | 1.4432 | 1.5049 | 1.5533 | 1.6289 | 1.7147 |
| | 0.6 | Present | 1.6381 | 1.8878 | 1.9635 | 2.0434 | 2.1330 | 2.2413 |
| | 0.8 | Present | 2.0240 | 2.3719 | 2.4645 | 2.5744 | 2.6819 | 2.8152 |
| | 1.0 | Present | 2.4315 | 2.8750 | 2.9861 | 3.129 | 3.2525 | 3.4119 |

**Table 9:** The bi-axial non-dimensional critical buckling load $\bar{\lambda}_{cr}$ of the simply supported sandwich FG square microplate with *a*/*h*=10

| *n* | *l*/*h* | Theory | $\bar{\lambda}_{cr}$ | | | | | |
|---|---|---|---|---|---|---|---|---|
| | | | 1-0-1 | 2-1-2 | 2-1-1 | 1-1-1 | 2-2-1 | 1-2-1 |
| 0 | 0 | Present | 6.5116 | 6.5116 | 6.5116 | 6.5116 | 6.5116 | 6.5116 |
| | | Anal-TSDT | 6.5025 | 6.5025 | 6.5025 | 6.5025 | 6.5025 | 6.5025 |
| | | Anal-SSDT | 6.5030 | 6.5030 | 6.5030 | 6.5030 | 6.5030 | 6.5030 |
| | | MF-HSDT | 6.5025 | 6.5025 | 6.5025 | 6.5025 | 6.5025 | 6.5025 |
| | | IGA-TSDT | 6.5025 | 6.5025 | 6.5025 | 6.5025 | 6.5025 | 6.5025 |
| | 0.2 | Present | 7.6543 | 7.6543 | 7.6543 | 7.6543 | 7.6543 | 7.6543 |
| | 0.4 | Present | 11.0791 | 11.0791 | 11.0791 | 11.0791 | 11.0791 | 11.0791 |

| | | | | | | | | |
|---|---|---|---|---|---|---|---|---|
| | 0.6 | Present | 16.7826 | 16.7826 | 16.7826 | 16.7826 | 16.7826 | 16.7826 |
| | 0.8 | Present | 24.7636 | 24.7636 | 24.7636 | 24.7636 | 24.7636 | 24.7636 |
| | 1.0 | Present | 35.0222 | 35.0222 | 35.0222 | 35.0222 | 35.0222 | 35.0222 |
| 1 | 0 | Present | 2.5881 | 2.9251 | 3.1023 | 3.2379 | 3.4805 | 3.7595 |
| | | Anal-TSDT | 2.5836 | 2.9200 | 3.0970 | 3.2324 | 3.4747 | 3.7533 |
| | | Anal-SSDT | 2.5842 | 2.9206 | 3.0973 | 3.2327 | 3.4749 | 3.7531 |
| | | MF-HSDT | 2.5392 | 2.8651 | 3.0368 | 3.1678 | 3.4027 | 3.6718 |
| | | IGA-TSDT | 2.5836 | 2.9200 | 3.0970 | 3.2324 | 3.4747 | 3.7533 |
| | 0.2 | Present | 3.2579 | 3.6872 | 3.8875 | 4.0613 | 4.3349 | 4.6596 |
| | 0.4 | Present | 5.2636 | 5.9690 | 6.2394 | 6.5273 | 6.8943 | 7.3568 |
| | 0.6 | Present | 8.5979 | 9.7620 | 10.1512 | 10.6278 | 11.1526 | 11.8449 |
| | 0.8 | Present | 13.2557 | 15.0603 | 15.6185 | 16.3574 | 17.1060 | 18.1205 |
| | 1.0 | Present | 19.2352 | 21.8619 | 22.6399 | 23.7144 | 24.7532 | 26.1824 |
| 5 | 0 | Present | 1.3316 | 1.5243 | 1.7051 | 1.7933 | 2.0600 | 2.3718 |
| | | Anal-TSDT | 1.3291 | 1.5213 | 1.7018 | 1.7898 | 2.0561 | 2.3673 |
| | | Anal-SSDT | 1.3300 | 1.5220 | 1.7022 | 1.7903 | 2.0564 | 2.3674 |
| | | MF-HSDT | 1.3234 | 1.5093 | 1.6860 | 1.7707 | 2.0308 | 2.3303 |
| | | IGA-TSDT | 1.3291 | 1.5213 | 1.7018 | 1.7898 | 2.0561 | 2.3674 |
| | 0.2 | Present | 1.6942 | 2.0421 | 2.2611 | 2.4139 | 2.7315 | 3.1196 |
| | 0.4 | Present | 2.7796 | 3.5892 | 3.9237 | 4.2678 | 4.7391 | 5.3552 |
| | 0.6 | Present | 4.5823 | 6.1524 | 6.6815 | 7.3389 | 8.0691 | 9.0629 |
| | 0.8 | Present | 7.0987 | 9.7201 | 10.5257 | 11.6127 | 12.7104 | 14.2297 |
| | 1.0 | Present | 10.3272 | 14.2857 | 15.4521 | 17.0812 | 18.6577 | 20.8491 |
| 10 | | Present | 1.2458 | 1.3759 | 1.5490 | 1.6006 | 1.8574 | 2.1441 |
| | | Anal-TSDT | 1.2436 | 1.3732 | 1.5460 | 1.5974 | 1.8538 | 2.1400 |
| | | Anal-SSDT | 1.2448 | 1.3742 | 1.5672 | 1.5973 | 1.5729 | 2.1909 |
| | | MF-HSDT | 1.2411 | 1.3654 | 1.5347 | 1.5842 | 1.8358 | 2.1090 |
| | | IGA-TSDT | 1.2436 | 1.3732 | 1.5460 | 1.5974 | 1.8538 | 2.1400 |
| | 0.2 | Present | 1.5383 | 1.8377 | 2.0525 | 2.1748 | 2.4873 | 2.8574 |
| | 0.4 | Present | 2.4147 | 3.2174 | 3.5582 | 3.8900 | 4.3700 | 4.9893 |
| | 0.6 | Present | 3.8730 | 5.5036 | 6.0560 | 6.7299 | 7.4916 | 8.5226 |
| | 0.8 | Present | 5.9119 | 8.6859 | 9.5380 | 10.6799 | 11.8407 | 13.4425 |
| | 1.0 | Present | 8.5311 | 12.7589 | 14.0007 | 15.7315 | 17.4116 | 19.7413 |

**Table 10:** The first five non-dimensional natural frequencies $\bar{\omega}$ of the simply supported sandwich square microplate with $n$=1 and $h_b - h_c - h_t = 2$ ? ?

| $n$ | $l/h$ | Method | Modes | | | | |
|---|---|---|---|---|---|---|---|
| | | | 1 | 2 | 3 | 4 | 5 |
| 1 | 0 | Present | 1.3009 | 3.1619 | 3.1619 | 4.9151 | 6.0650 |
| | | Anal-3D | 1.3018 | 3.1588 | 3.1588 | 4.9166 | 6.0405 |
| | | IGA-TSDT | 1.3001 | 3.1492 | 3.1492 | 4.8941 | - |
| | 0.2 | Present | 1.4606 | 3.5555 | 3.5556 | 5.5377 | 6.8376 |
| | 0.4 | Present | 1.8585 | 4.5323 | 4.5329 | 7.0768 | 8.7446 |
| | 0.6 | Present | 2.3769 | 5.7998 | 5.8012 | 9.0666 | 11.2055 |
| | 0.8 | Present | 2.9525 | 7.2034 | 7.2059 | 11.2643 | 13.9203 |
| | 1.0 | Present | 3.5575 | 8.6764 | 8.6801 | 13.5673 | 16.7631 |
| 10 | 0 | Present | | | | | |
| | | Anal-3D | 0.9404 | 2.2862 | 2.2862 | 3.5647 | 4.3844 |
| | | IGA-TSDT | 0.9430 | 2.3003 | 2.3003 | 3.5969 | - |
| | 0.2 | Present | 1.0906 | 2.6711 | 2.6711 | 4.1823 | 5.1806 |
| | 0.4 | Present | 1.4432 | 3.5338 | 3.5341 | 5.5366 | 6.8546 |
| | 0.6 | Present | 1.8878 | 4.6153 | 4.6161 | 7.2261 | 8.9379 |
| | 0.8 | Present | 2.3719 | 5.7873 | 5.7889 | 9.0498 | 11.1817 |
| | 1.0 | Present | 2.8750 | 7.0013 | 7.0040 | 10.9338 | 13.4963 |

## 5 Conclusion

A size-dependent HSDT meshfree model was presented for bending, free vibration and buckling analyses of FG microplates. The method retained one material length scale parameter and can capture the size effect. Material properties as Young's modulus, Poison's ratio and density mass varied the plate thickness according to the rule of mixture. The discrete system equations were obtained by employing the principle of virtual work and the MKI meshfree method. The present model can degenerate into the classical HSDT model when ignoring the material length scale parameter. For fully clamped boundary conditions, the normal slopes can be directly imposed by allocating zero values to the corresponding displacements at the boundary nodes and its adjacent nodes. By this way, it is not necessary to require additional variables in comparison with the traditional FEM. The effects of geometries, boundary conditions, aspect ratios, power index and material length-scale parameters on the displacement, natural frequency and critical buckling load of isotropic and sandwich FG microplates were studied. Numerical results indicated that a reduction of displacement and an increase of natural frequency as well as critical buckling load within the presence of size effects were conducted. It also shows that the stiffness of FG microplates were raised with respect to an increase of size effects. Besides, the results derived from the present and classical models were almost identical when the plate thickness was much far larger than the material length scale parameter.

Through numerical results, it shows that the present approach provided stable and accurate solutions in comparison with other methods.

**Acknowledgement:** This research is funded by Ho Chi Minh City Open University under grant number QT-16-1-32.

**References**

**Alinaghizadeh, F.; Shariati, M.; Fish J.** (2017): Bending analysis of size-dependent functionally graded annular sector microplates based on the modified couple stress theory. *Applied Mathematical Modelling*, vol. 44, pp. 540-556.

**Amiri, F.; Millán, D.; Shen, Y.; Rabczuk, T.; Arroyo, M.** (2014): Phase-field modeling of fracture in linear thin shells. *Theoretical and Applied Fracture Mechanics*, vol. 69, pp. 102-109.

**Ansari, R.; Norouzzadeh, A.** (2016): Nonlocal and surface effects on the buckling behavior of functionally graded nanoplates: An isogeometric analysis. *Physical E: Low-Dimensional Systems and Nanostructures*, vol. 84, pp. 84-97.

**Ansari, R.; Rajabiehfard, R.; Arash, B.** (2010): Nonlocal finite element model for vibrations of embedded multilayered graphene sheets. *Computational Materials Science*, vol. 49, no. 4, pp. 831-838.

**Askari, A. R.; Tahani, M.** (2015): Analytical determination of size-dependent natural frequencies of fully clamped rectangular microplates based on the modified couple stress theory. *Journal of Mechanical Science and Technology*, vol. 29, no. 5, pp. 2135-2145.

**Eshraghi, I.; Dag, S.; Soltani, N.** (2016): Bending and free vibrations of functionally graded annular and circular micro-plates under thermal loading. *Composite Structures*, vol. 137, pp. 196-207.

**Gao, X. L.; Huang, J. X.; Reddy, J. N.** (2013): A non-classical third-order shear deformation plate model based on a modified couple stress theory. *Acta Mechanica*, vol. 224, no. 11, pp. 2699-2718.

**Guo, J.; Chen, J.; Pan, E.** (2016): Analytical three-dimensional solutions of anisotropic multilayered composite plates with modified couple-stress effect. *Composite Structures*, vol. 153, pp. 321-331.

**Guo, J.; Chen, J.; Pan, E.** (2017): Free vibration of three-dimensional anisotropic layered composite nanoplates based on modified couple-stress theory. *Physica E: Low-dimensional Systems and Nanostructures*, vol. 87, pp. 98-106.

**He, L.; Lou, J.; Zhang, E.; Wang, Y.; Bai, Y.** (2015): A size-dependent four variable refined plate model for functionally graded microplates based on modified couple stress theory. *Composite Structures*, vol. 130, pp. 107-115.

**Jomehzadeh, E.; Noori, H. R.; Saidi, A. R.** (2011): The size-dependent vibration analysis of micro-plates based on a modified couple stress theory. *Physica E: Low-Dimensional Systems and Nanostructures*, vol. 43, no. 4, pp. 877-883.

**Ke, L. L.; Wang, Y. S.; Yang. J.; Kitipornchai, S.** (2012): Free vibration of size-dependent Mindlin microplates based on the modified couple stress theory. *Journal of Sound and Vibration*, vol. 331, no. 1, pp. 94-106.

**Kim, J.; Reddy, J. N.** (2013): Analytical solutions for bending, vibration, and buckling of FGM plates using a couple stress-based third-order theory. *Composite Structures*, vol. 103, pp. 86-98.

**Koiter, W. T.** (1964): Couple stresses in the theory of elasticity, I and II. *Nederl Akad Wetensch Process Series B*, vol. 67, pp. 17-44.

**Lam, D.; Yang, F.; Chong, A.; Wang, J.; Tong, P.** (2003): Experiments and theory in strain gradient elasticity. *Journal of the Mechanics and Physics of Solids*, vol. 51, no. 8, pp. 1477-1508.

**Lei, J.; He, Y.; Zhang, B.; Liu, D.; Shen, L. et al.** (2015): A size-dependent FG micro-plate model incorporating higher-order shear and normal deformation effects based on a modified couple stress theory. *International Journal of Mechanical Sciences*, vol. 104, pp. 8-23.

**Li, Q.; Lu, V.; Kou, K.** (2008): Three-dimensional vibration analysis of functionally graded material sandwich plates. *Journal of Sound and Vibration*, vol. 311, no. 1-2, pp. 498-515.

**Lou, J.; He, L.; Du, J.** (2015): A unified higher order plate theory for functionally graded microplates based on the modified couple stress theory. *Composite Structures*, vol. 133, pp. 1036-1047.

**Ma, H. M.; Gao, X. L.; Reddy, J. N.** (2011): A non-classical Mindlin plate model based on a modified couple stress theory. *Acta Mechanica*, vol. 220, no. 1-4, pp. 217-235.

**Ma, L. S.; Wang, T. J.** (2004): Relationship between axisymmetric bending and buckling solutions of FGM circular plates based on third-order plate theory and classical plate theory. *International Journal of Solids and Structures*, vol. 41, no. 1, pp. 85-101.

**Mindlin, R. D.; Eshel, N. N.** (1968): On first strain-gradient theories in linear elasticity. *International Journal of Solids and Structures*, vol. 4, no. 1, pp. 109-124.

**Mindlin, R. D.; Tiersten, H. F.** (1962): Effects of couple-stresses in linear elasticity. *Archive for Rational Mechanics and Analysis*, vol. 11, no. 1, pp. 415-448.

**Mindlin, R. D.** (1964): Micro-structure in linear elasticity. *Archive for Rational Mechanics and Analysis*, vol. 16, no. 1, pp. 51-78.

**Mirsalehi, M.; Azhari, M.; Amoushahi, H.** (2015): Stability of thin FGM microplate subjected to mechanical and thermal loading based on the modified couple stress theory and spline finite strip method. *Aerospace Science and Technology*, vol. 47, pp. 356-366.

**Natarajan, S.; Chakraborty, S.; Thangavel, M.; Bordas, S.; Rabczuk, T.** (2012): Size-dependent free flexural vibration behavior of functionally graded nanoplates. *Computational Materials Science*, vol. 65, pp. 74-80.

**Neves, A. M. A.; Ferreira, A. J. M.; Carrera, E.; Cinefra, M.; Roque, C. M. C. et al.** (2013): Static, free vibration and buckling analysis of isotropic and sandwich functionally graded plates using a quasi-3D higher-order shear deformation theory and a meshless technique. *Composite Part B: Engineering*, vol. 44, no. 1, pp. 657-674.

**Nguyen, K. D.; Nguyen-Xuan, H.** (2015): An isogeometric finite element approach for three-dimensional static and dynamic analysis of functionally graded material plate structures. *Composite Structures*, vol. 132, pp. 423-439.

**Nguyen, N. T.; Hui, D.; Lee, J.; Nguyen-Xuan, H.** (2015): An efficient computational approach for size-dependent analysis of functionally graded nanoplates. *Computer Methods in Applied Mechanics and Engineering*, vol. 297, pp. 191-218.

**Nguyen, N. T.; Thai, C. H.; Nguyen-Xuan, H.** (2016): A novel computational approach for functionally graded isotropic and sandwich plate structures based on a rotation-free meshfree method. *Thin-Walled Structures*, vol. 107, pp. 473-488.

**Nguyen-Thanh, N.; Zhou, K.; Zhuang, X.; Areias, P.; Nguyen-Xuan, H. et al.** (2017): Isogeometric analysis of large-deformation thin shells using PHT-splines for multiple-patch coupling. *Computer Methods in Applied Mechanics and Engineering*, vol. 316, pp. 1157-1178.

**Nguyen-Xuan, H.; Tran, V. L.; Thai, H. C.; Kulasegaram, S.; Bordas, S. P. A.** (2014): Isogeometric analysis of functionally graded plates using a refined plate theory. *Composites Part B: Engineering*, vol. 64, pp. 222-234.

**Nguyen, X. H.; Nguyen, N. T.; Wahab, M. A.; Bordas, S. P. A.; Nguyen-Xuan, H. et al.** (2017): A refned quasi-3D isogeometric analysis for functionally graded microplates based on the modifed couple stress theory. *Computer Methods in Applied Mechanics and Engineering*, vol. 313, pp. 904-940.

**Phadikar, J. K.; Pradhan, S. C.** (2010): Variational formulation and finite element analysis for nonlocal elastic nanobeams and nanoplates. *Computational Materials Science*, vol. 49, no. 3, pp. 492-499.

**Phan-Dao, H. H.; Thai, C. H.; Lee, J.; Nguyen-Xuan, H.** (2016): Analysis of laminated composite and sandwich plate structures using generalized layerwise HSDT and improved meshfree radial point interpolation method. *Aerospace Science and Technology*, vol. 58, pp. 641-660.

**Rabczuk, T.; Areias, P. M. A.; Belytschko, T.** (2007): A meshfree thin shell method for non-linear dynamic fracture. *International Journal for Numerical Methods in Engineering*, vol. 72, no. 5, pp. 524-548.

**Rabczuk, T.; Gracie, R.; Song, J. H.; Belytschko T.** (2010): Immersed particle method for fluid-structure interaction. *International Journal for Numerical Methods in Engineering*, vol. 81, no. 1, pp. 48-71.

**Reddy, J. N.** (2000): Analysis of functionally graded plates. *International Journal for Numerical Methods in Engineering*, vol. 47, no. 1-3, pp. 663-684.

**Roque, C. M. C.; Ferreira, A. J. M.; Reddy, J. N.** (2013): Analysis of Mindlin micro plates with a modified couple stress theory and a meshless method. *Applied Mathematical Modelling*, vol. 37, no. 7, pp. 4626-4633.

**Salehipour, H.; Nahvi, H.; Shahidi, A.; Mirdamadi, H. R.** (2017): 3D elasticity analytical solution for bending of FG micro/nanoplates resting on elastic foundation using modified couple stress theory. *Applied Mathematical Modelling*, vol. 47, pp. 174-188.

**Saidi, A. R.; Rasouli, A.; Sahraee, S.** (2009): Axisymmetric bending and buckling analysis of thick functionally graded circular plates using unconstrained third-order shear deformation plate theory. *Composite Structures*, vol. 89, no. 1, pp. 110-119.

**Sarrami-Foroushani, S.; Azharim, M.** (2016): Nonlocal buckling and vibration analysis of thick rectangular nanoplates using finite strip method based on refined plate theory. *Acta Mechanica*, vol. 277, no. 3, pp. 721-742.

**Thai, C. H.; Do, N. V. V.; Nguyen-Xuan, H.** (2016): An improved moving Kriging-based meshfree method for static, dynamic and buckling analysis functionally graded isotropic and sandwich plates. *Engineering Analysis with Boundary Elements*, vol. 64, pp. 122-136.

**Thai, C. H.; Ferreira, A. J. M.; Lee, J.; Nguyen-Xuan, H.** (2018): An efficient size-dependent computational approach for functionally graded isotropic and sandwich microplates based on modified couple stress theory and moving Kriging-based meshfree method. *International Journal of Mechanical Sciences*, vol. 142-143, pp. 322-338.

**Thai, C. H.; Ferreira, A. J. M.; Nguyen-Xuan, H.** (2018): Isogeometric analysis of size-dependent isotropic and sandwich functionally graded microplates based on modified strain gradient elasticity theory. *Composite Structures*, vol. 192, pp. 274-288.

**Thai, C. H.; Ferreira, A. J. M.; Nguyen-Xuan, H.** (2017): Naturally stabilized nodal integration meshfree formulations for analysis of laminated composite and sandwich plates. *Composite Structures*, vol. 178, pp. 260-276.

**Thai, C. H.; Ferreira, A. J. M.; Rabczuk, T.; Nguyen-Xuan, H.** (2018): A naturally stabilized nodal integration meshfree formulation for carbon nanotube-reinforced composite plate analysis. *Engineering Analysis with Boundary Elements*, vol. 92, pp. 136-155.

**Thai, C. H.; Ferreira, A. J. M.; Rabczuk, T.; Bordas, S. P. A.; Nguyen-Xuan, H.** (2014): Isogeometric analysis of laminated composite and sandwich plates using a new inverse trigonometric shear deformation theory. *European Journal of Mechanics-A/Solids*, vol. 43, pp. 89-108.

**Thai, C. H.; Ferreira, A. J. M.; Wahab, M. A.; Nguyen-Xuan, H.** (2018): A moving Kriging meshfree method with naturally stabilized nodal integration for analysis of functionally graded material sandwich plates. *Acta Mechanica*, vol. 229, no. 7, pp. 2997-3023.

**Thai, C. H.; Kulasegaram, S.; Tran, V. L.; Nguyen-Xuan, H.** (2014): Generalized shear deformation theory for functionally graded isotropic and sandwich plates based on isogeometric approach. *Computers & Structures*, vol. 141, pp. 94-112.

**Thai, C. H.; Nguyen, N. T.; Rabczuk, T.; Nguyen-Xuan, H.** (2016): An improved moving Kriging meshfree method for plate analysis using a refined plate theory. *Computer & Structures*, vol. 176, pp. 34-49.

**Thai, H. T.; Choi, D. H.** (2013): Size-dependent functionally graded kirchhoff and mindlin plate models based on a modified couple stress theory. *Composite Structures*, vol. 95, pp. 142-153.

**Thai, H. T.; Vo, T. P.** (2013): A size-dependent functionally graded sinusoidal plate model based on a modified couple stress theory. *Composite Structures*, vol. 96, pp. 376-383.

**Thai, H. T.; Kim, S. E.** (2013): A size-dependent functionally graded Reddy plate model based on a modified couple stress theory. *Composites Part B: Engineering*, vol. 45, no. 1, pp. 1636-1645.

**Thai, H. T.; Vo, P. T.; Nguyen, T. K.; Kim, S. E.** (2017): A review of continuum mechanics models for size-dependent analysis of beams and plates. *Composite Structures*, vol. 177, pp. 196-219.

**Toupin, R. A.** (1962): Elastic materials with couple-stresses, *Archive for Rational Mechanics and Analysis*, vol. 11, pp. 385-414.

**Trinh, L. C.; Vo, T. P.; Thai, H. T.; Mantari, J. L.** (2017): Size-dependent behaviour of functionally graded sandwich microplates under mechanical and thermal loads. *Composites Part B: Engineering*, vol. 124, pp. 218-241.

**Tsiatas, G. C.** (2009): A new Kirchhoff plate model based on a modified couple stress theory. *International Journal of Solids and Structures*, vol. 46, no. 13, pp. 2757-2764.

**Nguyen, T. N.; Ngo, T. D.; Nguyen-Xuan, H.** (2017): A novel three-variable shear deformation plate formulation: Theory and isogeometric implementation. *Computer Methods in Applied Mechanics and Engineering*, vol. 326, pp. 376-401.

**Yang, F.; Chong, A. C. M.; Lam, D. C. C.; Tong, P.** (2002): Couple stress based strain gradient theory for elasticity. *International Journal of Solids and Structures*, vol. 39, no. 10, pp. 2731-2743.

**Yin, L.; Qian, Q.; Wang, L.; Xia, W.** (2010): Vibration analysis of microscale plates based on modified couple stress theory. *Acta Mechanica Solida Sinica*, vol 23, no. 5, pp. 386-393.

**Zenkour, A. M.** (2005): A comprehensive analysis of functionally graded sandwich plates: Part 2 buckling and free vibration. *International Journal of Solids and Structures*, vol. 42, no. 18-19, pp. 5243-5258.

**Zhou, S. S.; Gao, X. L.** (2014): A nonclassical model for circular mindlin plates based on a modified couple stress theory. *Journal of Applied Mechanics*, vol. 81, no. 5, pp.1-8.

**Zhang, Y.; Lei, Z. X.; Zhang, L. W.; Liew, K. M.; Yu, J. L.** (2015): Nonlocal continuum model for vibration of single-layered graphene sheets based on the element-free kp-Ritz method. *Engineering Analysis with Boundary Elements*, vol. 56, pp. 90-97.